remote sensing

MDPI

Article

A Sentinel-2 Based Multi-Temporal Monitoring Framework for Wind and Bark Beetle Detection and Damage Mapping

Anna Candotti [1,2,*], Michaela De Giglio [1], Marco Dubbini [1] and Enrico Tomelleri [2]

[1] Department of History and Cultures (DiSCi)-Geography Section, University of Bologna, Via Guerrazzi 20, 40125 Bologna, Italy
[2] Faculty of Science and Technology, Free University of Bolzano, Piazza Università 5, 39100 Bolzano, Italy
* Correspondence: anna.candotti@natec.unibz.it

Abstract: The occurrence of extreme windstorms and increasing heat and drought events induced by climate change leads to severe damage and stress in coniferous forests, making trees more vulnerable to spruce bark beetle infestations. The combination of abiotic and biotic disturbances in forests can cause drastic environmental and economic losses. The first step to containing such damage is establishing a monitoring framework for the early detection of vulnerable plots and distinguishing the cause of forest damage at scales from the management unit to the region. To develop and evaluate the functionality of such a monitoring framework, we first selected an area of interest affected by windthrow damage and bark beetles at the border between Italy and Austria in the Friulian Dolomites, Carnic and Julian Alps and the Carinthian Gailtal. Secondly, we implemented a framework for time-series analysis with open-access Sentinel-2 data over four years (2017–2020) by quantifying single-band sensitivity to disturbances. Additionally, we enhanced the framework by deploying vegetation indices to monitor spectral changes and perform supervised image classification for change detection. A mean overall accuracy of 89% was achieved; thus, Sentinel-2 imagery proved to be suitable for distinguishing stressed stands, bark-beetle-attacked canopies and wind-felled patches. The advantages of our methodology are its large-scale applicability to monitoring forest health and forest-cover changes and its usability to support the development of forest management strategies for dealing with massive bark beetle outbreaks.

Keywords: forests; spruce bark beetle; windstorms; drought; remote sensing; Sentinel-2; spectral signatures; vegetation indices; supervised image classification; forest-cover change detection

Citation: Candotti, A.; De Giglio, M.; Dubbini, M.; Tomelleri, E. A Sentinel-2 Based Multi-Temporal Monitoring Framework for Wind and Bark Beetle Detection and Damage Mapping. *Remote Sens.* **2022**, *14*, 6105. https://doi.org/10.3390/rs14236105

Academic Editors: Bogdan Andrei Mihai, Mihai Nita and Marcel Torok

Received: 10 November 2022
Accepted: 29 November 2022
Published: 1 December 2022

1. Introduction

Due to ongoing global climate change, forest ecosystems are increasingly exposed to unfavourable environmental conditions, such as droughts and cold spells. Such changes are linked to contemporaneously rising temperatures and changing precipitation patterns [1]. At the same time, the frequency of disturbances such as major windthrows and snow damage exposes forest ecosystems to an increase in the frequency and severity of biotic damage [1]. Thus, native and alien insect, fungal and nematode infestations are expected to be a major threat to European forests in the future [1]. In this context, the homogeneity of even-aged monoculture stands of Norway spruce (*Picea abies*) is a favourable condition for the diffusion of the European spruce bark beetle (*Ips typographus*) [2]. Increasing stress conditions of such forest stands have supported the uncontrolled growth of the bark beetle population to epidemic proportions to the point that the insect has already destroyed more forested areas than any other natural disturbance [2,3]. Spruce bark beetle infestations are affected by rising temperatures due to the exothermic physiology of the insects and the drought sensitivity of the defence system of trees [4]. Female beetles drill egg galleries under the bark. Later, larvae emerge and feed in the phloem before changing

into pupae. The adults may move on to another host two to five weeks after the attack. The larvae feed in the phloem after hatching and pupate beneath the bark [1]. Each year, up to three generations are possible [1]. The successful beetle colonisation of a healthy tree is typically fatal, because hundreds of beetle attacks destroy the inner bark and disrupt nutrient transport to the roots [1]. If this increase in mortality persists for a more extended period, large patches of forest (Figure 1) could be affected with a consequently altered forest structure and composition and losses of biodiversity and ecosystem service provision (e.g., hydrological regulation and carbon storage capacity) [5]. To prevent massive outbreaks and to minimise economic losses induced by a range of cascading impacts on markets, such as oversupply and decreasing timber prices, the early detection of infestations is crucial, that is, before the infestation is visible on the ground [6]. Management measures successfully applied in the past are becoming inefficient under a warmer climate, particularly in forests dominated by Norway spruce because of their lower resistance to drought stress. On the other hand, forests managed for diversity have shown lower disturbance rates [7].

Figure 1. An example of combined abiotic (wind-felled patches) and biotic (bark beetle infestations) disturbances in Norway spruce stands at a site located in the Carnic Alps (picture taken from Mount Tersadia, 1960 m a.s.l.).

A prerequisite for effective management is understanding forest damage's spatial distribution and severity. From a forestry perspective, detecting outbreaks at the initial stage is the most important, as the management aims to preclude a mass outbreak by sanitation harvesting [8]. The phenology of bark beetle attacks can be divided into three stages: green, red and grey attacks, with varying degrees of visibility [9,10]. These stages were named after the characteristic foliage colour, which is related to the time since the phloem damage occurred [9,10].

Infested trees in a managed forest are traditionally located during field surveys, but the method is laborious and hardly applicable to large or inaccessible areas [11]. An important new management strategy might be to reduce risks by looking at the whole landscape configuration rather than at single stands to account for measures that foster forest resilience at ecosystem level [12]. Remote sensing data are useful for detecting and monitoring areas infested by spruce bark beetles, as they provide global, spatially continuous and periodic data on vegetation conditions [13]. Remote sensing data can also reduce costs associated with field observations, as there are many freely available data sources with

global coverage and regular revisit times, such as Sentinel-2 [14]. The availability of high-quality (i.e., cloud-free) Sentinel-2 images is an important prerequisite for the successful monitoring of bark beetle damage dynamics, as they show high variability in space and time [15]. Accurate estimates of leaf pigments, nitrogen, dry matter and water content from remote sensing can assist in determining the vegetation's physiological status and serve as bioindicators of vegetation stress [16,17,18]. Einzmann et al. [19] found that in an artificially induced stress experiment on Norway spruce, the spectra of stressed trees differed significantly from the mean of the control trees. In contrast, the control tree spectral signature did not change over time. Compared to the mean of the control trees, both the needle and the canopy reflectance of artificially stressed trees increased in the visible (mainly red) and SWIR ranges, while a decrease was observed in the Near-Infrared (NIR) range. Furthermore, a slight decrease in the Red-Edge Inflection Point (REIP) was observed. The primary and secondary effects of water content on leaf reflectance showed that the sensitivity of leaf reflectance to water content is greatest in spectral bands in the SWIR region [18]. These changes are caused by a typical reaction to vitality losses and cell structure alterations when chlorophyll and leaf water are reduced. In addition to altered leaf optical properties, needle loss affects canopy-scale spectral signatures [19]. Both the changes in the photosynthetic activity of green leaves and water content variations triggered by bark beetle can be detected in early infestation stages using imaging spectroscopy. The resolution of Sentinel-2 imagery was demonstrated to be advantageous for such purposes [20]. An overall accuracy of 67% in detecting the bark beetle green attack stage with Sentinel-2 data was obtained for 2016 in the Bavarian Forest National Park without relying on field data and only on the visual interpretation of aerial photographs taken in the year following the attack [20]. Reflectance changes in infested Norway spruce trees were observable, especially in the Red-Edge and SWIR regions, as well as in vegetation indices calculated from those bands, such as the Normalised Difference Red-Edge Index (NDREI) and the Normalised Difference Water Index (NDWI), for both leaf and canopy levels [20,21]. Research in 2020 showed that Sentinel-2 data were able to accurately distinguish areas with bark beetle disturbances and to detect the individual phases of the recovery mode of the forest vegetation using the Normalised Difference Vegetation Index (NDVI), the Normalised Difference Moisture Index (NDMI) and Tasselled Cap Wetness (TCW) during the period of 2017 to 2019 in the Low Tatras National Park (Slovakia) and the Sumava National Park (Czech Republic) [22]. The reflectance of healthy forest vegetation was higher in the NIR band than in the SWIR band; however, the SWIR reflectivity was higher in the case of bark beetle disturbances. This aspect played an important role, as the SWIR bands responded sensitively in the case of the degradation of the forest [22]. Spectral changes in healthy and attacked spruce monoculture stands within a single vegetation season were monitored in the Bohemian–Moravian Highlands (Czech Republic) using a dense time series of Sentinel-2 satellite observations to identify the most sensitive spectral bands and vegetation indices for the early detection of bark beetle infestation [15]. The highest potential for separation between healthy and infestation classes was observed for the Red, Red-Edge and SWIR regions of the spectrum, with an overall accuracy of 78%. In this study [15], NIR bands seemed less appropriate for early bark beetle detection, despite the recent evidence from Abdullah et al. [20] pointing to significant differences in leaf-level NIR spectra between healthy and infested trees. Spectral indices using Red-Edge and Short-Wave Infrared might be potentially useful to detect infestations even earlier than indices based solely on the VIS/NIR region [15,23]. Approaches based on multi-temporal spectral analysis have proven to be the most effective in detecting bark beetle infestations at an early stage with Sentinel-2 data [14–16,22–24].

Herein, we propose a new multi-temporal framework for regional-scale wind and bark beetle damage mapping from Sentinel-2 imagery and field surveys. In doing this, we first evaluated the detection of early stages of bark beetle attacks on Norway spruce stands over four years (2017–2020) by tracking their within-season changes in canopy reflectance. Individual spectral bands and vegetation indices were used to develop a supervised

image classification model in order to separate classes of healthy, stressed, "red_attack" stage or windstorm-damaged stands over an area of 1,000,000 ha, of which 120,000 ha is covered by Norway spruce. Lastly, the results were validated with field reference data and implemented for the analysis of forest-cover change by post-classification change detection over the time series concerning both spruce bark beetle infestations and windstorm damage.

2. Materials and Methods

2.1. Study Area

The chosen study site for bark beetle detection and the analysis of forest-cover change (2017–2020) is located at the border between Italy, Austria and Slovenia in the Friulian Dolomites, Carnic and Julian Alps and the Carinthian Gailtal (Figure 2). In Friuli Venezia Giulia, Norway spruce is the main forest species, covering about 66,100 ha and scattered in seven main types of mixed and pure forests. The other common diffused tree species are European beech, Silver fir, and Black and Scots pines [25]. Typical pure and even-aged spruce forests grow on fertile soils from 1000 to 1500 m a.s.l., and non-native even-aged spruce forests, sometimes mixed with natural spruce reforestation (secondary stands), grow from 800 to 1600 m a.s.l. in abandoned pastures. Several areas have been replanted with Norway spruce owing to market-oriented reforestation management of the XX century. There has been recent low-altitude spruce reforestation with pure and even-aged spruce plantations, which normally grow in small stands from 200 to 800 m a.s.l in areas that are dominated by broadleaved species [26]. In addition, on the Carinthian side of the study area, Norway spruce, followed by Silver fir, Black and Scots pines, European beech and Larch are the main tree species [27]. For the purpose of this study, only sites in the study area with Norway spruce stands (pure or mixed) were considered (Figure 2).

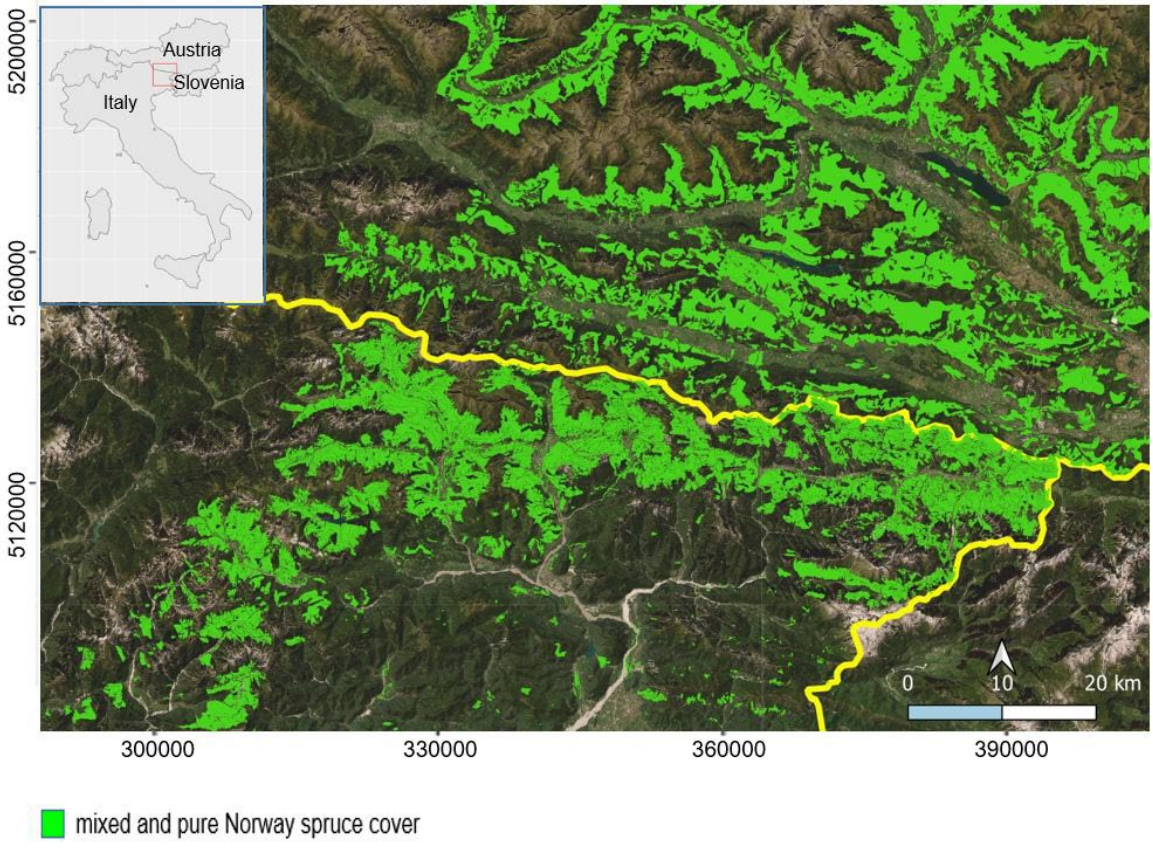

Figure 2. Location of the study area, with polygons in green representing mixed and pure Norway spruce stands and state borders in yellow (ESRI Satellite base map). Reference system: WGS84-UTM33N.

The mountain areas of the study area are characterised, at lower latitudes, by high annual precipitation, ranging from 2700 to 3200 mm per year, while in the internal alpine area, it only amounts to ca. 1500 mm. The average annual air temperature ranges between 6 and 10 °C [28,29]. Regarding the yearly average climate conditions of the study region, 2018 was very hot and dry, having a mean temperature of 13 °C in mountain areas, while 2019 and 2020 had a mean temperature of 10°C [30–32]. Nevertheless, both 2019 and 2020 were characterised by an annual temperature anomaly of 1°C for 2019 and of 2.4 °C for 2020 compared to the last two decades [31,32]. Spring average precipitation strongly impacts bark beetle population development [33]. While the spring months of 2018 showed a mean increase in rainfall of 20–40% compared to the average values in 1961–2010 [30,34], the spring (including June) of 2019 was 20–50% drier than usual [31]. March and April 2020 were even 60–80% drier than the reference period [32].

The Vaia Storm

The Vaia storm hit the northeastern part of Italy and southern Austria between the 28 and 29 October 2018, with winds exceeding 200 km/h and intense rainfall [35]. It caused extensive forest damage in 494 Italian municipalities, destroying or severely damaging forests over an area of about 42,500 ha, with the damage estimated to cover 9.6 million cubic metres across an area of 42,500 ha [35]. For the Friuli Venezia Giulia region, the local forest service provided estimates of the forest damage using aerial photographs and ground surveys, which estimated that a surface extending 3700 ha was damaged and that the volume affected by the storm was 780,000 cubic meters [35]. In Carinthia, Vaia caused 1.5 million cubic metres of damaged wood [30]. Vaia mainly affected pure and mixed Norway spruce stands, as their roots are relatively superficial and prone to uprooting [36]. In forest stands where trees were more diversified in age and species, the devastating effects of the wind were more restricted, with better resistance due to the different morphology of the root system [36].

2.2. Data

We utilised satellite imagery to detect forest stress due to bark beetle attacks and to monitor forest change over the study period. For this purpose, we made use of Sentinel-2A and Sentinel-2B images in the form of Level-2A products (atmospherically corrected to bottom-of-atmosphere reflectance) [37]. We collected Sentinel-2 tiles with the R package "getSpatialData" (version 0.1.0), selecting images with less than 10% cloud cover. Images were cropped to the area of interest, and bands with an original resolution of 20 m × 20 m (B05, B06, B07, B11 and B12) were resampled to 10 m × 10 m pixels. We did not use bands with a 60 m spatial resolution (B01 and B09) because they are mainly relevant for atmospheric corrections [38]. The dataset was collected with a monthly time step for the period from July to September from the years 2017 to 2020. We included May based on data availability due to higher cloud cover in spring (Table 1). The timeframe was chosen according to the bark beetle life cycle phenology in the study area, which begins in May for overwintered beetles, expands to July for the second generation and ends in September. The attacked trees are initially stressed ("green_attack") and later encounter a browning process, the timing of which is diverse, depending on the time of the year at which the trees were initially attacked. The culmination of such a browning process is commonly called a "red_attack". Stands attacked in May usually show visible symptoms such as needle loss and initial discolouration in July, while those infested in summer show "red_attack" symptoms in the following spring [39]. Forest cover masks were obtained from the Copernicus Land Monitoring Service [40], which provides the tree cover density (TCD) and dominant leaf type (DLT), indicating a broadleaf or needle-leaf majority. These datasets are available with 20 m resolution starting from the year 2018. Secondly, we merged these datasets with the forest cover polygons—which include the dominant tree species—from the Autonomous Region Friuli Venezia Giulia and Land Kärnten to increase the accuracy and to include the specific forest cover type.

Table 1. Sentinel-2 data.

Number	Date	Data
1	20 June 2017	Sentinel-2 L2A
2	2 August 2017	Sentinel-2 L2A
3	29 August 2017	Sentinel-2 L2A
4	6 May 2018	Sentinel-2 L2A
5	30 July 2018	Sentinel-2 L2A
6	17 August 2018	Sentinel-2 L2A
7	28 September 2018	Sentinel-2 L2A
8	24 May 2019	Sentinel-2 L2A
9	30 June 2019	Sentinel-2 L2A
10	27 August 2019	Sentinel-2 L2A
11	21 September 2019	Sentinel-2 L2A
13	07 July 2020	Sentinel-2 L2A
14	29 July 2020	Sentinel-2 L2A
15	15 September 2020	Sentinel-2 L2A

We gathered information about the bark beetle population counts from pheromone traps in Friuli Venezia Giulia for the years from 2017 to 2020 (Figure 3). This dataset, provided by the Regional Agency for Rural Development (ERSA FVG), contains the location and altitude of the trap, its installation date, captures per week and total captures. Bark beetle captures by pheromone traps in the northern part of the region showed an increase in the population and diffusion in 2019, especially related to areas covered by wind-felled trees [41]. On the Austrian side of the study area, we used the PHENIPS model and trap captures from the Austrian Federal Forest Office (BFW) [42]. Additionally, we included polygons of sites damaged by bark beetle infestations with information about the stand species and the age and volume of damaged trees and polygons representing wind-felled sites from the Vaia storm of 2018, located during field surveys and provided by the Regional Forestry Service (Friuli Venezia Giulia) and the Carinthian Institute for Geographic Information Systems (KAGIS) (Figure 3). Orthophotos from 2017–2020 provided by the Regional Infrastructure of Environmental and Territorial Data (Irdat FVG) [43] were used for the photointerpretation of wind-felled areas and sites affected by bark beetle damage. We extracted the topographic parameters from a digital elevation model (Global Digital Elevation Model from the NASA Earth Data Portal) [44] for the areas affected by bark beetle attacks and wind damage.

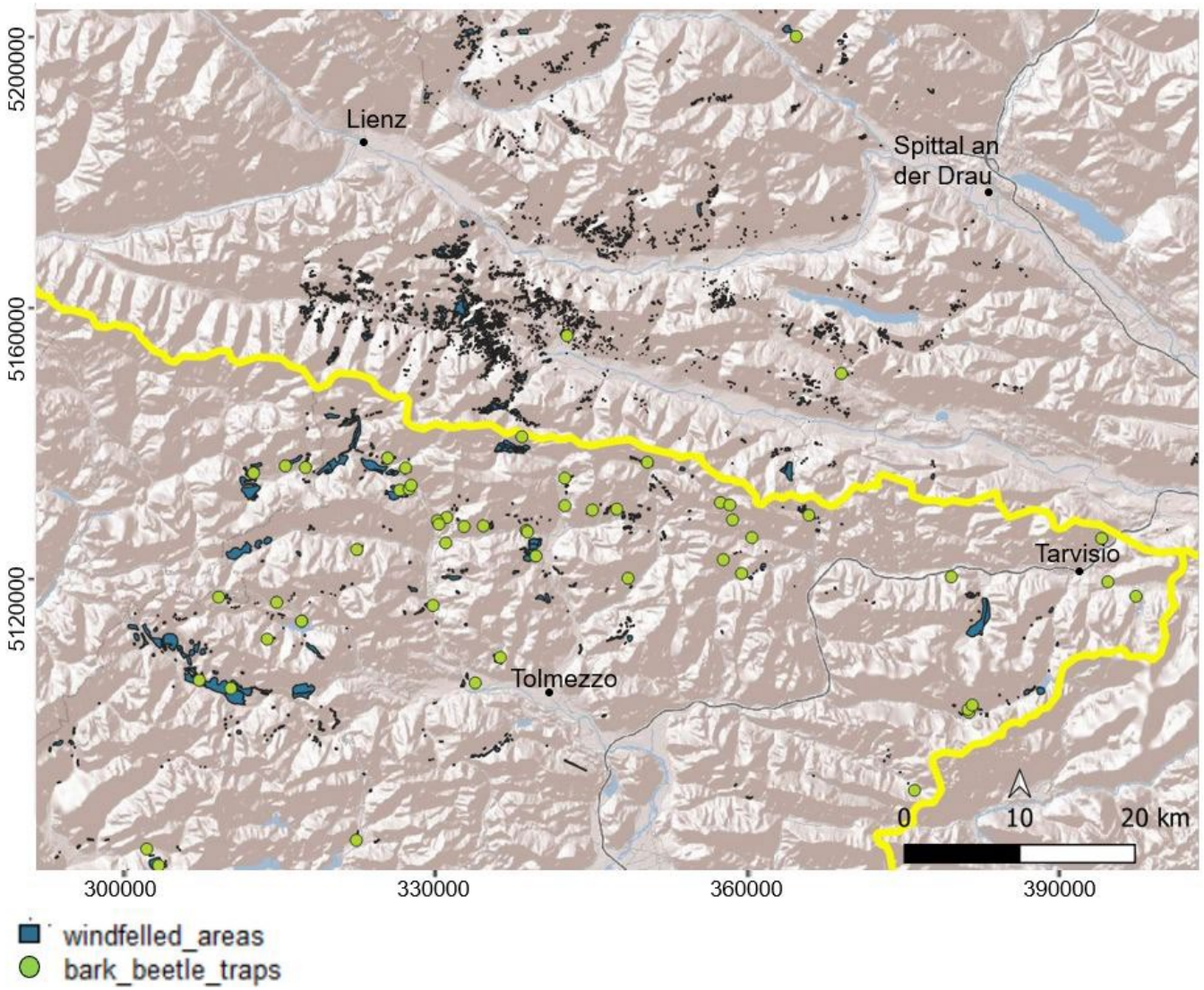

Figure 3. Reference data distribution over the study area showing the location of bark beetle pheromone traps and wind-felled patches (ESRI Shaded Relief base map). Reference system: WGS84-UTM33N.

Additionally, we exploited the Soil Water Index (SWI) from the Copernicus Global Land Service [40] to quantify the moisture conditions. Moreover, we gathered land surface temperature (LST) data from the Sentinel-3 mission from the Copernicus Open Access Hub [45]. We carried out the analysis for this study in the R programming language (version 4.1.2).

2.3. Methods

Cloud masks were applied to every scene according to the native cloud cover information of Sentinel-2 Level 2-A products [37] (Figure 4). Such masks do not account for shadowed areas, which can be easily distinguished by unusually low reflectance in the visible part of the spectrum. Consequently, such areas were treated as a separate training site class for each dataset during the classification process.

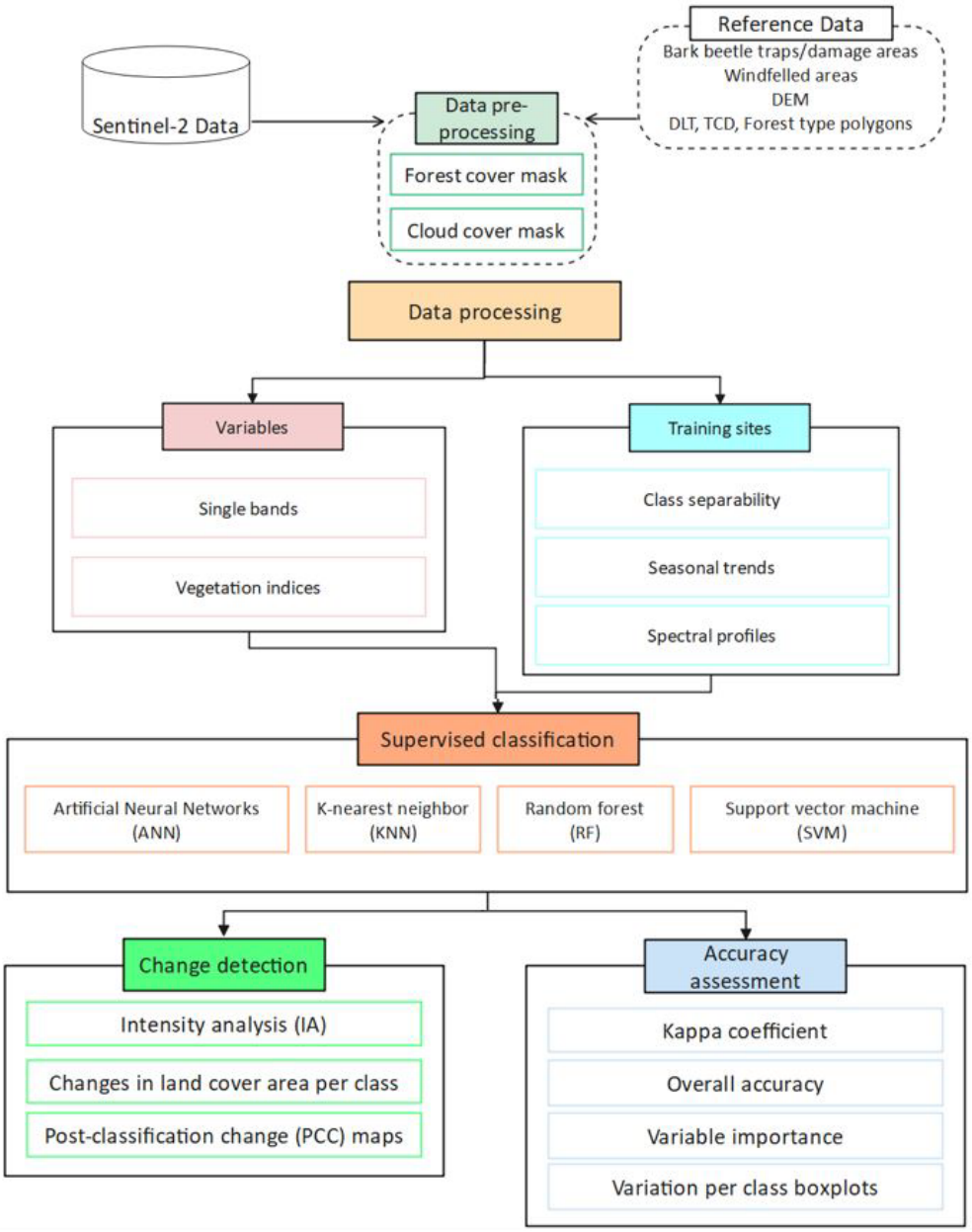

Figure 4. Workflow diagram.

2.3.1. Single Bands and Vegetation Indices

Single-band pixel values from Sentinel-2 images were analysed for each available acquisition date (Figure 4) considering ground-truth reference data and photointerpretation from RGB and false-colour products. Especially the reflectance trends of the NIR (B08) and SWIR (B12) bands were taken into account because they are the most sensitive ones to chlorophyll decreases (B08 band) and water stress/lower absorption rates (B12 band) [15,21]. Training data, i.e., training polygons drawn for the classes of healthy, stressed and "red attack" stage canopies from 2020, were used to extract spectral profiles for both bands (B08 and B12) in order to quantify the variables' separability and seasonal changes over time.

From the Sentinel-2 imagery, we extracted the time series of vegetation indices (Figure 4 and Table 2) for the growing seasons of 2019 and 2020 to detect forest health changes using training polygons from 2020.

Table 2. Vegetation indices tested in this study.

Index	Sentinel-2 Bands	Application
NDWI	NIR, SWIR2	Water content
NDVI	NIR, Red	Greenness
DWSI	NIR, Red	Greenness
NMDI	NIR, Green, SWIR1, Red	Water content
NDRS	Red, SWIR1	Greenness, water content
REIP	Red, RedEdge2, RedEdge1	Greenness, water content
NDREI1	RedEdge2, RedEdge1	Chlorophyll, biomass
NDREI2	RedEdge3, RedEdge1	Chlorophyll, biomass
RENDVI	Red, RedEdge1, RedEdge2	Greenness, biomass
TCW	Blue, Green, Red, NIR, SWIR1, SWIR2	Water content

The indices were chosen based on the bands' sensitivity to stress-induced variations in chlorophyll content (VIS), biomass (NIR) and water content (SWIR). For the green-attack stage detection, mainly water-content-based indices are suitable, such as the Normalised Difference Water Index (NDWI, Equation (1)), which is dimensionless with a range of ±1, where high values indicate high leaf water content and high vegetation cover. This index is handy in early stress detection. It allows the more accurate mapping of temporal changes, as it exhibits faster feedback than the Normalised Difference Vegetation Index (NDVI, Equation (2)) for decreasing leaf water content [46,47]. Additionally, the NDWI is more robust to atmospheric influences, as atmospheric aerosol scattering effects are stronger in the VIS spectral wavelengths [46,47]:

$$NDWI = \frac{(NIR - SWIR2)}{(NIR + SWIR2)} \quad (1)$$

$$NDVI = \frac{(NIR - Red)}{(NIR + Red)} \quad (2)$$

Disease Water Stress Index (DWSI, Equation (3)) was calculated, as it proved to be able to detect changeable climatic conditions, especially the impact of drought on forest ecosystems, in which case DWSI decreases. DWSI values range between 0 and 2.5 for forests, according to a previous study. In the case of pure conifers, there is a distinct difference in the DWSI index for dry sites, especially for the first part of the vegetation period, from April to July [48]:

$$DWSI = \frac{(NIR - Green)}{(SWIR1 + Red)} \quad (3)$$

The Normalised Multi-band Drought Index (NMDI, Equation (4)) was adopted for detecting vegetation water by using three channels centred near 860 nm, 1640 nm and 2130 nm. By combining information from multiple NIR and SWIR channels, NMDI enhances the sensitivity to drought severity and is well suited to estimate the water content for both soil and vegetation [47]. NMDI values are within the range of 0.7 to 1 when soil moisture is less than 0.1, which means dry soil conditions. NMDI values are around 0.6 when soil is under intermediate moisture conditions. When NMDI is less than 0.6, the soil is under wet conditions. Lower NMDI values indicate the increasing severity of vegetation drought [47].

$$NMDI = \frac{(NIR - (SWIR1 - SWIR2))}{(NIR + (SWIR1 + SWIR2))} \quad (4)$$

The Normalised Distance Red and SWIR (NDRS, Equation (5)) vegetation index, which was recently implemented for the early detection of forest stress from spruce bark beetle attacks, was also used in this research [24]:

$$NDRS = \frac{(DRS - DRS'\min)}{(DRS'max - DRS'\min)} \quad (5)$$

where

$$DRS = \sqrt{(Red)^2 + (SWIR1)^2} \quad (6)$$

DRS'max and DRS'min are the ranges of the DRS values for all spruce pixels in the image, and a threshold of 0.5 is applied to classify pixels as stressed or healthy if lower [24].

Red-Edge-based vegetation indices were calculated for bark beetle detection, too. Among them is the REIP (Equation (7)), as with increasing stress, the abrupt transition that is typically seen between the visible and NIR bands in the Red-Edge range in green vegetation begins to shift towards shorter wavelengths [49]. The Normalised Difference Red-Edge Index (NDREI, Equation (8)) can be applied to estimate chlorophyll concentrations, minimising the effects of background soil reflectance, with values below 0.5 indicating stress conditions [23]:

$$REIP = \frac{0.705 + 0.35\,(\frac{Red + RedEdge3}{2 - RedEdge1})}{RedEdge2 - RedEdge1} \quad (7)$$

$$NDREI1 = \frac{(RedEdge2 - RedEdge1)}{(RedEdge2 + RedEdge1)} \quad (8)$$

$$NDREI2 = \frac{(RedEdge3 - RedEdge1)}{(RedEdge3 + RedEdge1)} \quad (9)$$

The Red-Edge Normalised Difference Vegetation Index (RENDVI, Equation (10)), also called Red-Edge NDVI or NDVI 705, which was used to assess post-fire regeneration and based on Red and Red-Edge bands in another study [50], was compared with other indexes in this study. Both bands B04 and B05 and bands B04 and B06 were used. In the following formula, R represents the bottom-of-atmosphere (BOA) reflectance observed by the satellite sensor:

$$RENDVI = \frac{(R750nm - R705nm)}{(R750nm + R705nm)} \quad (10)$$

This index proved to be useful, as it considers a narrower waveband at the edge of the chlorophyll absorption feature (e.g., 705 nm). NDVI 705 is more affected by the chlorophyll content when compared to the NDVI, and typical applications include precision agriculture, forest monitoring, forest fires and vegetation stress detection [51].

Additionally, Tasselled Cap Wetness (TCW, Equation (11)) was calculated to further distinguish between disturbed and undisturbed forest areas with the specific parameters from the Index Database [52]:

$$TCW = 0.1509 \times B02 + 0.1973 \times B03 + 0.3279 \times B04 + 0.3406 \times B08 - 0.7112 \times B11 - 0.4572 \times B12 \quad (11)$$

TCW has previously proven to be helpful for the detection of forest stands attacked by bark beetles, showing negative values for infested forest sites [22].

2.3.2. Supervised Classification of Multi-Temporal Imagery

We first performed supervised image classification (Figure 3) to assign each pixel to a particular forest class of interest ("healthy", "stressed", "red_attack" or "vaia") based on the statistical characteristics of the reflectance values of the training samples. Four non-parametric machine learning methods were used: Random Forest (RF), Support Vector Machine (SVM), Artificial Neural Networks (ANNs) and k-Nearest Neighbours (KNN). Training polygons were manually selected based on RGB and false-colour composites, as

well as single-band reflectance values and reference data (trap captures, areas damaged by bark beetles, wind-felled areas and orthophotos) for each dataset. The training polygons were based only on reference data (Figure 4) available at the time of the respective image acquisition to avoid taking a retrospective approach through ground-truth information gathered afterwards, as it would have compromised the green-attack stage detection. At least ten polygons per class, 30 m × 30 m each (3 × 3 pixels), were drawn. We chose the size of the training dataset based on a rule of thumb according to which a subset size of at least ten times the number of bands used during the classification (in this case, 9) has to be considered for each training class [53].

The training polygons were sampled for each Sentinel-2 dataset and split into a training (70%) and a test (30%) dataset. Spectral signatures were extracted for each date to detect a reflectance trend for each class. The classification algorithms were trained using both single bands and vegetation indices as explanatory variables, as in a recent study [15]. Variable importance was calculated in order to evaluate which explanatory variables were the most significant during the classification process in distinguishing between classes based on their reflectance values. The classifications were finally assessed with confusion matrices, overall accuracy and the kappa coefficient (Figure 4).

2.3.3. Post-Classification Forest-Cover Change Detection

We carried out post-classification change detection (PCC) by Intensity Analysis (IA) to quantitatively analyse Land-Use Capability (LUC) maps at several time steps using cross-tabulation matrices, where each matrix summarises the LUC change at each time interval (Figure 4). IA evaluates in three levels the deviation between the observed change intensity and the hypothesised uniform change intensity. As a result of this, each level details information provided by the previous analysis level. Firstly, the interval level indicates how the size and rate of change vary across time intervals. Secondly, the category level examines how the size and intensity of gross losses and gross gains in each category vary across categories for each time interval. Thirdly, the transition level determines how the size and intensity of a category's transitions vary across the other categories available for that transition. At each level, the method tests for the stationarity of patterns across time intervals [54]. The discrete variables obtained from the results of supervised classification were used for this purpose. The R-package "OpenLand" (version 1.0.2) was used to calculate the number of times a pixel changed during the analysed period. A raster with the number of changes in the pixel value and a table containing the areal percentage of every pixel value (number of changes) were obtained. Further, the calculation of differences in the frequencies of pixels assigned per class for each dataset was performed. Changes in land cover area per class were plotted to visualise changes in forest cover before and after the Vaia storm and how it affected bark beetle infestations. Finally, we used classification maps from 2017 to 2020 to evaluate two focus areas showing relevant changes in forest cover and health.

3. Results

3.1. Single Bands and Vegetation Indices Reflectance Values

The results obtained from single-band change detection over time using training data from 2020 showed that in the NIR band (B08) (Figure 5A) and in the SWIR band (B12) (Figure 5B), there is a significant variation in reflectance within areas damaged by bark beetles compared to the reflectance values of healthy forest stands. On the other hand, the differences between healthy and stressed stands are more significant in the B08 band, with values of the stressed sites being more similar to the spectral profile of stands in the bark beetle "red_attack" stage than to the healthy ones (Figure 5A). In addition, healthy stands displayed seasonal variation in reflectance, with values increasing until July (2019) or August (2020) and decreasing from summer to early autumn (September 2019 and 2020). Considering the seasonal reflectance of the summer months in the B08 band, while healthy

stands witnessed a significant increase in NIR reflectance, the stands of stressed and "red_attack" sites only showed a slight rise in reflectance (Figure 5A). In the B12 band, forest stands in the bark beetle "red_attack" stage can clearly be distinguished by higher reflectance values, while healthy and stressed stands had very similar spectral responses for both seasons.

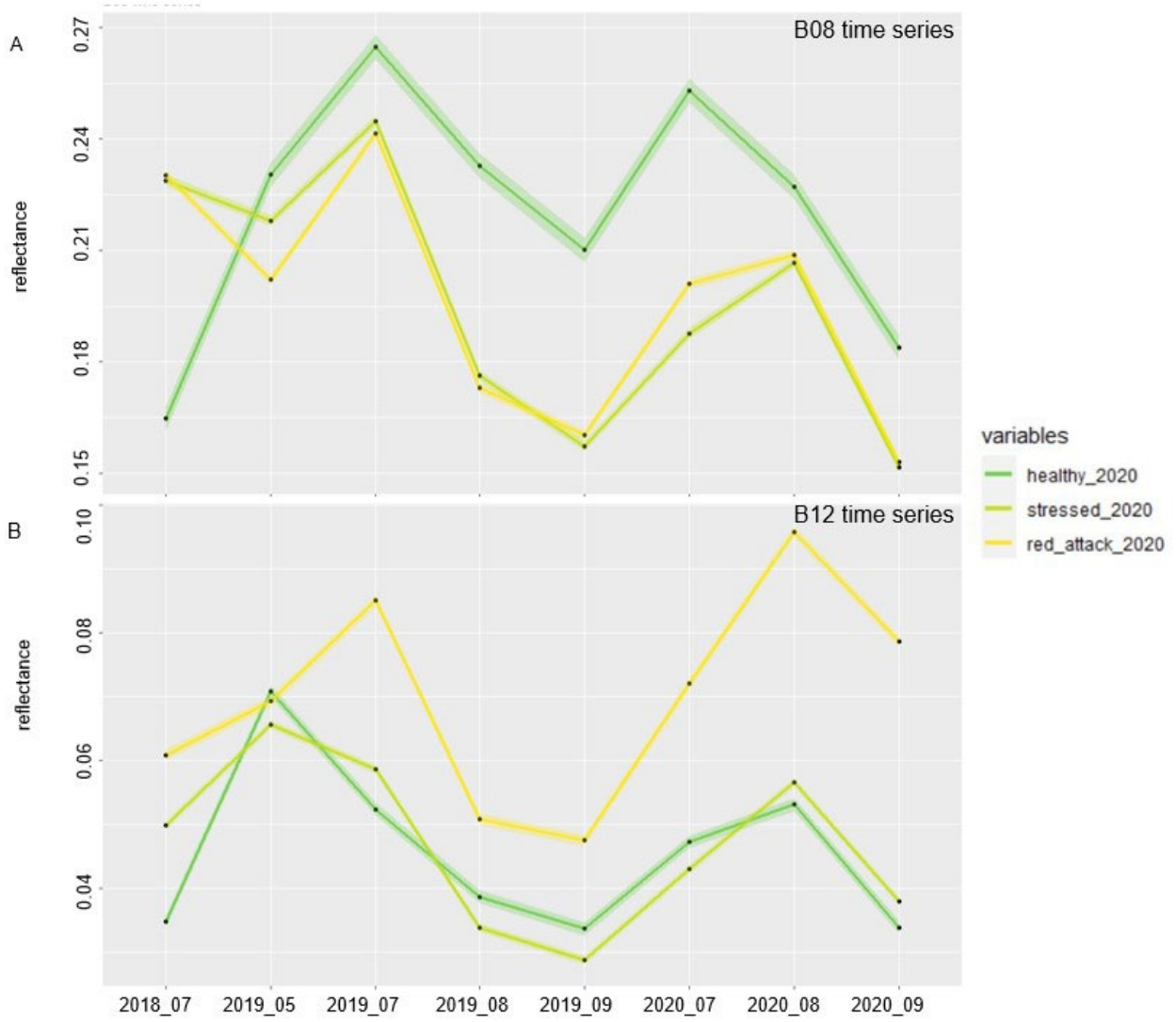

Figure 5. Mean seasonal B08 (**A**) and B12 (**B**) band reflectance (line) and standard error from 95% CI (confidence band) in a time series from 2018 to 2020 for healthy, stressed and red-attack stage canopies using training data from 2020.

Nevertheless, a slight increase in reflectance was observed in stressed stands beginning in August 2020 compared to the values of healthy stands (Figure 5B). Stands identified as being in the bark beetle red-attack stage in 2020 already showed significantly deviating values in 2019 compared to the healthy canopies for both bands (Figure 5A,B). Forest areas selected as stressed according to training data from 2020 exhibited similar spectral responses for both 2019 and 2020, however, with overall lower values in 2020 in the B08 band (Figure 5A) and higher reflectance in August and September 2020 in the B12 band (Figure 5B).

The vegetation indices NDWI, DWSI, NMDI, NDRS, NDREI2 and TCW, among the ten that were later considered for classification, were found to be suitable to successfully distinguish between healthy and stressed or damaged forest stands. The most frequently

used band for these indices is the B12 band. The reported indices further rely on the B08 band, B05, B06 and B07 (Red-Edge bands), B03 (green band) and/or B04 (red band). For all vegetation indices and for both considered seasons, the values of healthy and stressed stands are more similar to each other compared to forests undergoing "red_attack" bark beetle infestation, which show very significant differences (Figure 6). For normalised indices (NDWI, NDMI and NDREI2), in all cases, healthy stands displayed the highest values, followed by samples from stressed stands, with the lowest values for stands in the bark beetle "red-attack" stage (Figure 6A,B,E). NDRS was found to have very similar values for healthy and stressed stands, while forest stands in the "red_attack" stage resulted in significantly higher values (Figure 6D). TCW exhibited positive values for healthy stands, values between 0 and −250 for stressed stands and an even lower range (between −125 and −625) for "red_attack" stage canopies (Figure 6F). NDWI, NMDI, DWSI and TCW showed the largest difference between healthy and stressed pixels (Figure 6A,B,C,F). While healthy and stressed stands showed very similar seasonal trends for both seasons, stands already in the "red-attack" stage in 2020 showed the most significant decreases beginning in July 2020 for NDWI, NMDI, DWSI and NDREI2 compared to the values of 2019 (Figure 6A,B,C,E). However, both stressed and "red_attack" stage canopies from 2020 already showed deviating values in 2019 compared to the reflectance of healthy crowns (Figure 6). The seasonal trajectories showed reflectance changes in absolute values from one year to another independently of bark beetle infestations (healthy forest stands were also affected), which indicates that an absolute threshold of discrimination between classes cannot be applied and that the specific seasonal reflectance of healthy forest stands should instead be used as a reference baseline to differentiate between the variables (Figure 6).

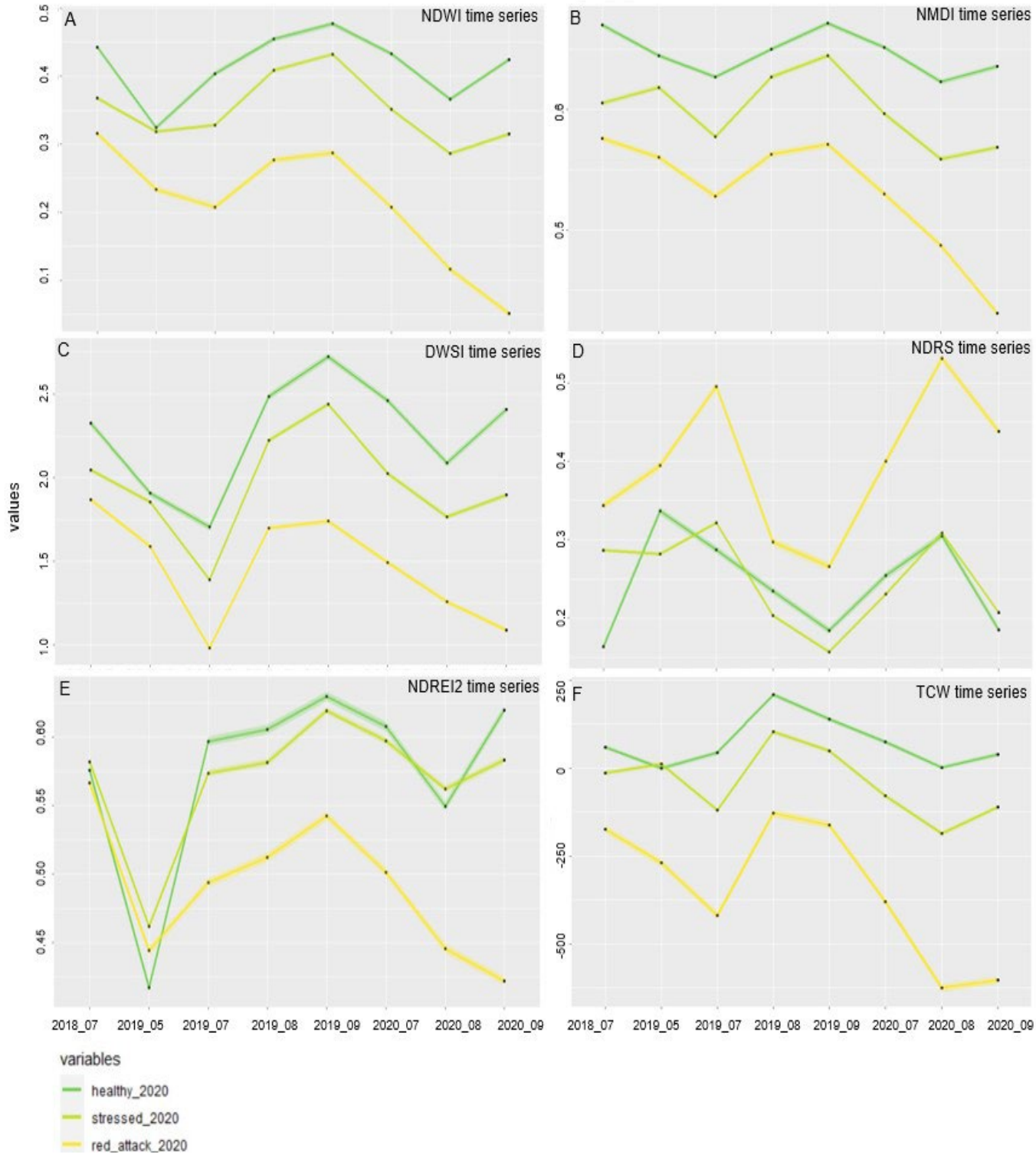

Figure 6. Mean seasonal reflectance trends (line) and standard error from 95% CI (confidence band) of vegetation indices (NDWI (**A**), NMDI (**B**), DWSI (**C**), NDRS (**D**), NDREI2 (**E**) and TCW (**F**) from 2018 to 2020 with training data from 2020 for the classes of healthy, stressed and "red_attack" stage canopies.

3.2. Supervised Classification

3.2.1. Spectral Signatures

Spectral signatures were extracted for the chosen classes of each dataset in order to identify changes in reflectance between bands for each class (Figure 7). For the visible

region of the electromagnetic spectrum, an increase in both green (B03) and red (B04) was found for the "red_attack" stage class compared to the reflectance values of healthy stands, while the Red-Edge bands (B06 and B07) showed a significant decrease (Figure 7A,C). In the SWIR bands (B11 and B12), an increase in reflectance is shown for the "red_attack" class (Figure 7A,C). The "stressed" class showed a decrease in reflectance for the green band (B03) towards values of the red band (B04) (Figure 7A,C). The Red-Edge region (B05, B06 and B07) is characterised by lower reflectance values compared to those of the "healthy" class, while the SWIR bands (B11 and B12) are characterised by similar values to those of healthy stands (Figure 7A,C). The "stressed" class was also the one with the lowest variation for all bands (Figure 7B,D).

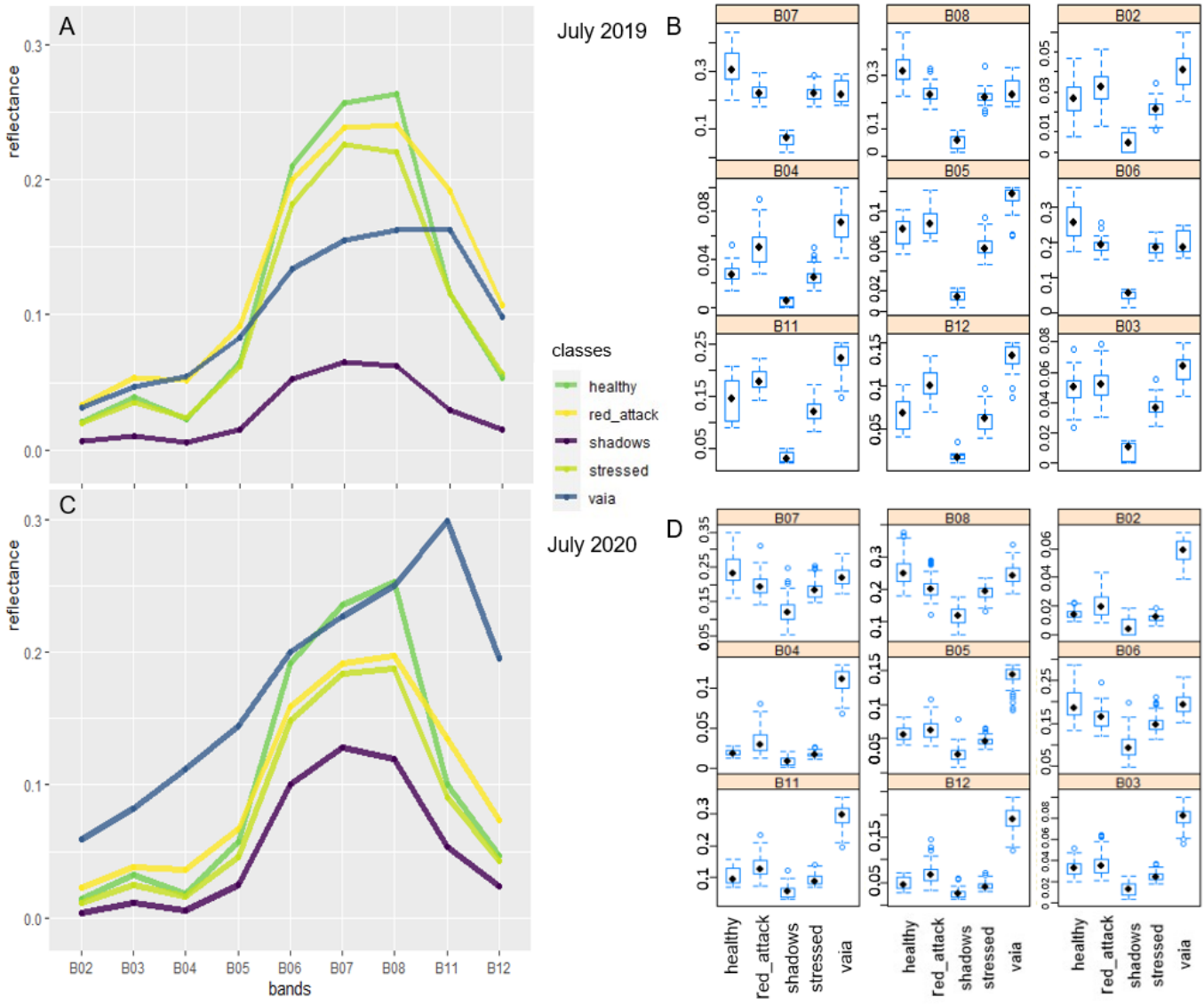

Figure 7. Mean spectral profiles from training site classes for each band (**A**) and (**C**) and variation per class for each band (**B**) and (**D**) in July 2019 and July 2020 for forest cover classes of healthy vegetation, stands in the bark beetle "red-attack" stage, shadows, stressed forest stands and Vaia-storm-related windthrows.

3.2.2. Maps of Damage

Supervised classification was performed over the entire area of interest at once. For demonstration purposes, we focus on two cropped areas to highlight the classification

results (Figure 8). The maps were compared with validation ground surveys and the visual interpretation of orthophotos from 2020 provided by Irdat FVG [43].

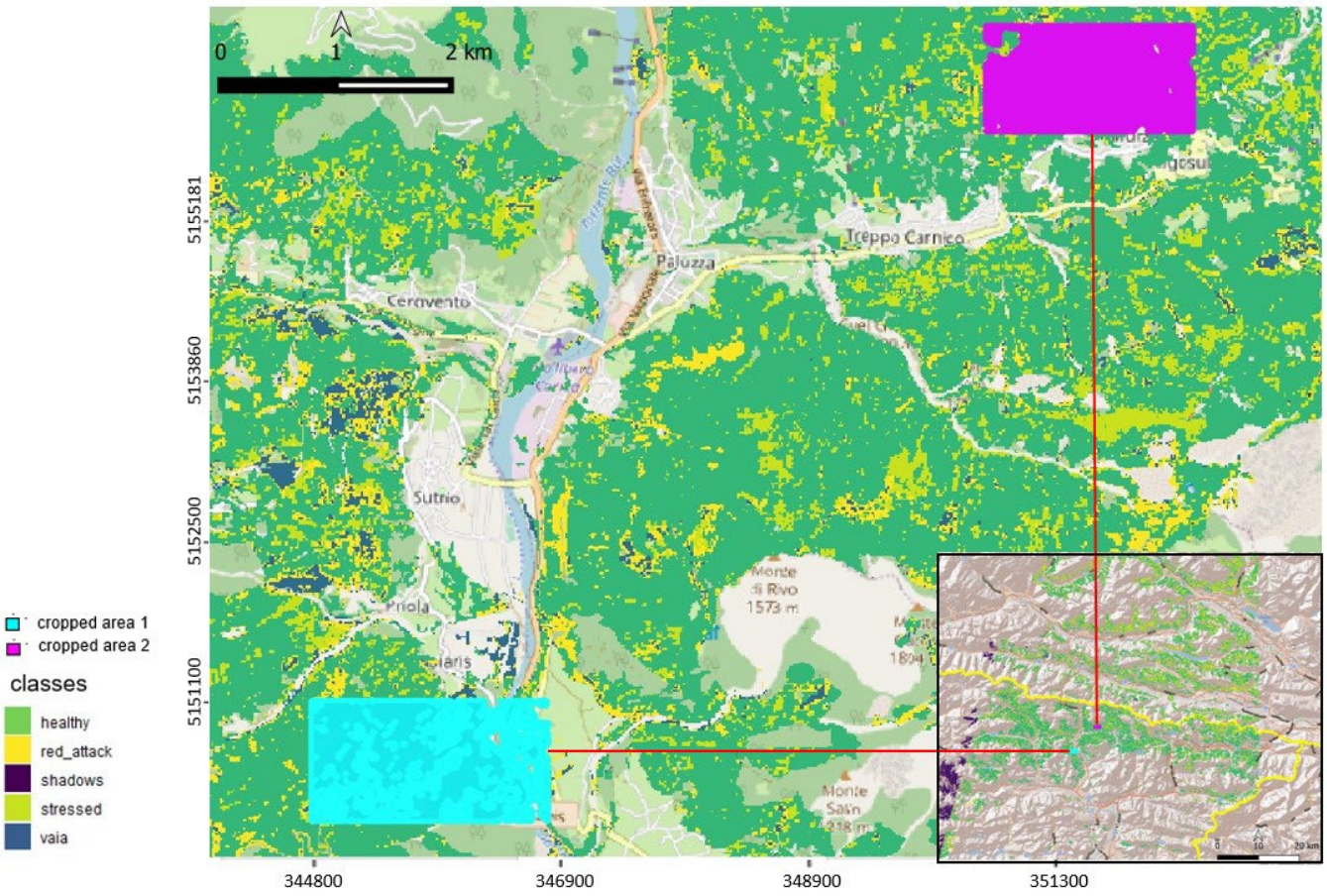

Figure 8. Location of two cropped areas in the study area selected to visualise classification results and changes in forest cover and health based on classes of healthy forest stands, stressed vegetation, stands in the bark beetle "red-attack" stage and Vaia-storm-related windthrows (OpenStreetMap base map). Reference System: WGS84-UTM33N.

Forest stands in cropped area nr. 1 already showed conditions of stress and the "red_attack" stage in June 2017 (Figure 9A). The sites detected as stressed in June 2017 (Figure 9A) were classified as "red_attack" stage stands in the classification map of July 2018 (Figure 9B). The area was already suffering from bark beetle infestations before the Vaia storm occurred. However, a significant increase in damage can be seen in the "after Vaia" situation in 2019 and 2020, especially beginning in September 2019 (Figure 9E) and July 2020 (Figure 9, F). Some of the stands that were already stressed in May 2019 (Figure 9C) changed into the "red_attack" stage in July 2019 (Figure 9D), and others changed in September 2019 (Figure 9E). Not all of the stands detected as stressed turned into the "red_attack" stage, but all of those which eventually turned out to have been infested by bark beetles had previously been classified as stressed. The bark beetle spread that occurred after the Vaia storm progressed along forest edges and/or in proximity to windfelled patches (Figure 9D,E,F). At the same time, according to the classification results (Figure 9), forest stands that suffered damage from Vaia were located along forest edges and/or next to forest stands that were already suffering from bark beetle infestations before the storm occurred.

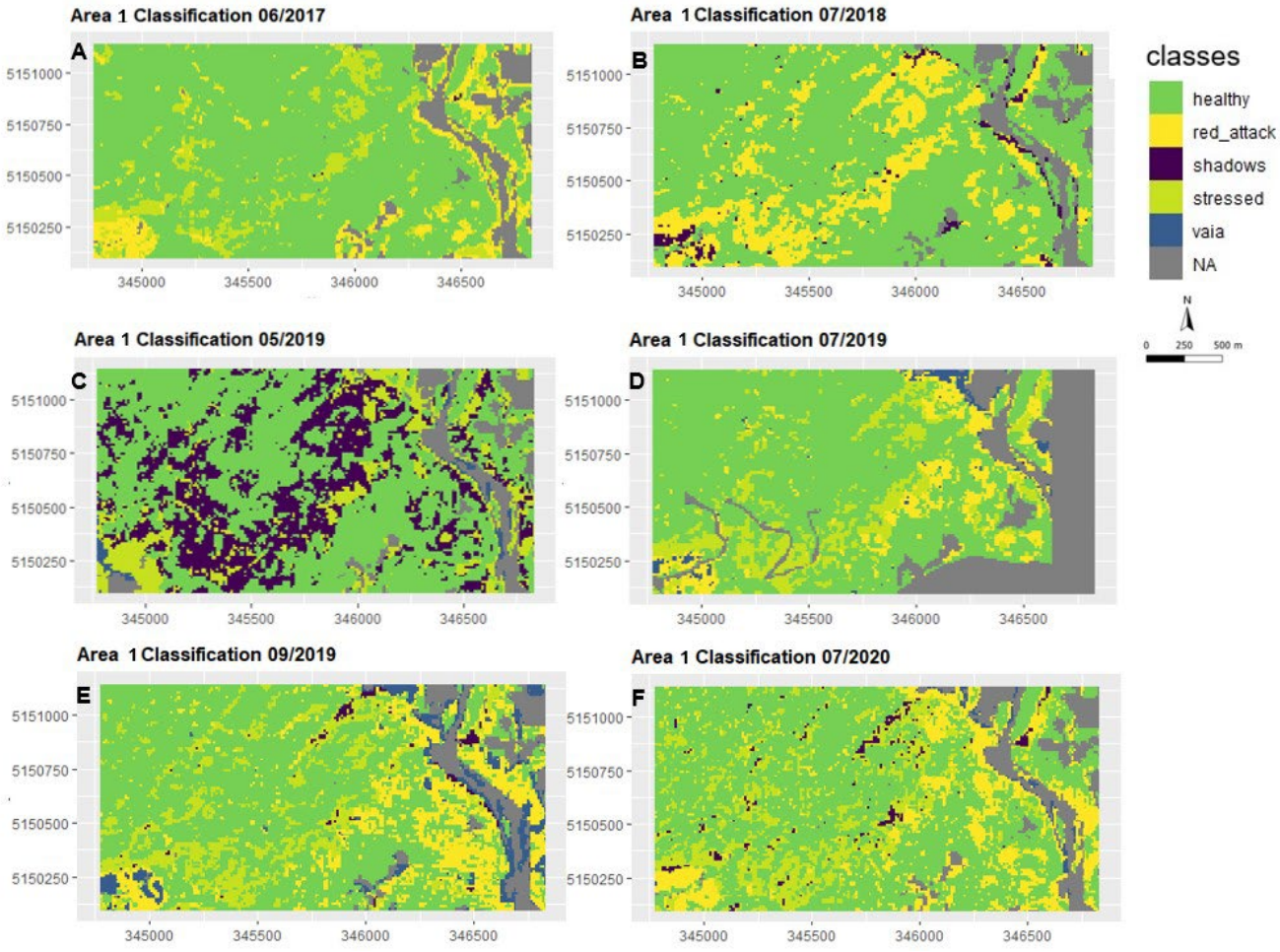

Figure 9. Classification maps of cropped area 1 from 2017 to 2020 (June 2017 (**A**), July 2018 (**B**), May 2019 (**C**), July 2019 (**D**), September 2019 (**E**) and July 2020 (**F**) according to forest cover classes ("healthy", "red_attack", "shadows", "stressed" and "vaia"). Reference System: WGS84-UTM33N.

As in cropped area nr. 1, the forest stands of cropped area 2 (Figure 10) also already showed conditions of stress and the "red_attack" stage in June 2017 (Figure 10A). The sites detected as stressed in June 2017 (Figure 10A) were classified as "red_attack" stage stands in the classification map of July 2018 (Figure 10B). Some of the canopies detected as stressed in May 2019 (Figure 10C) turned into the "red_attack" stage class as early as in July 2019 (Figure 10D), while most of them changed class in September 2019 (Figure 10E) or even in the following season (Figure 10F). Orthophoto details from 2020 showed that several forest stands located near wind-felled areas (top-right corner of the orthophoto details) were classified as stressed in 2019 (Figure 10C–E) and turned into the "red_attack" stage in July 2020 (Figure 10F). According to the classification results, bark beetle infestations generally intensified after the Vaia storm, especially in 2020, two years after the event (Figure 10F), and spread in proximity to wind-felled patches (Figure 10E).

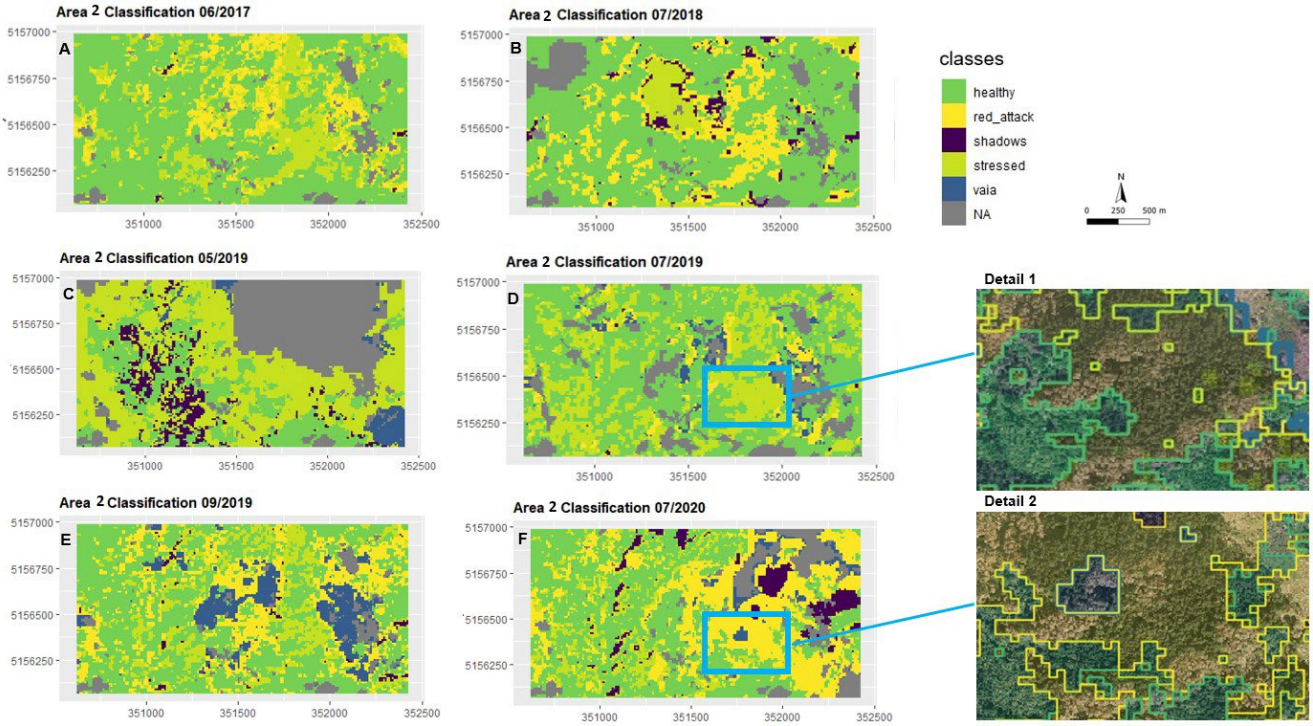

Figure 10. Classification maps of cropped area 2 (June 2017 (**A**), July 2018 (**B**) , May 2019 (**C**), July 2019 (**D**), September 2019 (**E**) and July 2020 (**F**)) according to forest cover classes ("healthy", "red_attack", "shadows", "stressed" and "vaia") and details showing orthophotos from 2020 with a spatial resolution of 10 cm provided by IRDAT. The orthophotos were overlayed by classification products in the form of polygons and transparent rasters. Reference system: WGS84-UTM33N.

The overall accuracies of all supervised classifications reported varied between 0.8 and 1, with kappa values between 0.7 and 1 (Appendix A Table A1). The variable importance slightly varied between the different classification algorithms, of which ANN and RF were found to be the most suitable for forest health detection and forest-cover change detection. The most important variables for ANN classification were the Red-Edge bands (B06 and B07) and the green band (B03), as well as vegetation indices containing Red-Edge bands, such as NDREI1, NDREI2 and REIP, as well as TCW (Figure 11B,D; Appendix A Figure A1B,D and A2B,D). The RF algorithm mainly relied on the Red-Edge band (B06), the NIR band (B08) and the NDRS index containing the red (B04) and SWIR (B12) bands, as well as on vegetation indices containing Red-Edge bands (NDREI2 and REIP) (Figure 11A,C; Appendix A Figure A1A,C and A2A,C).

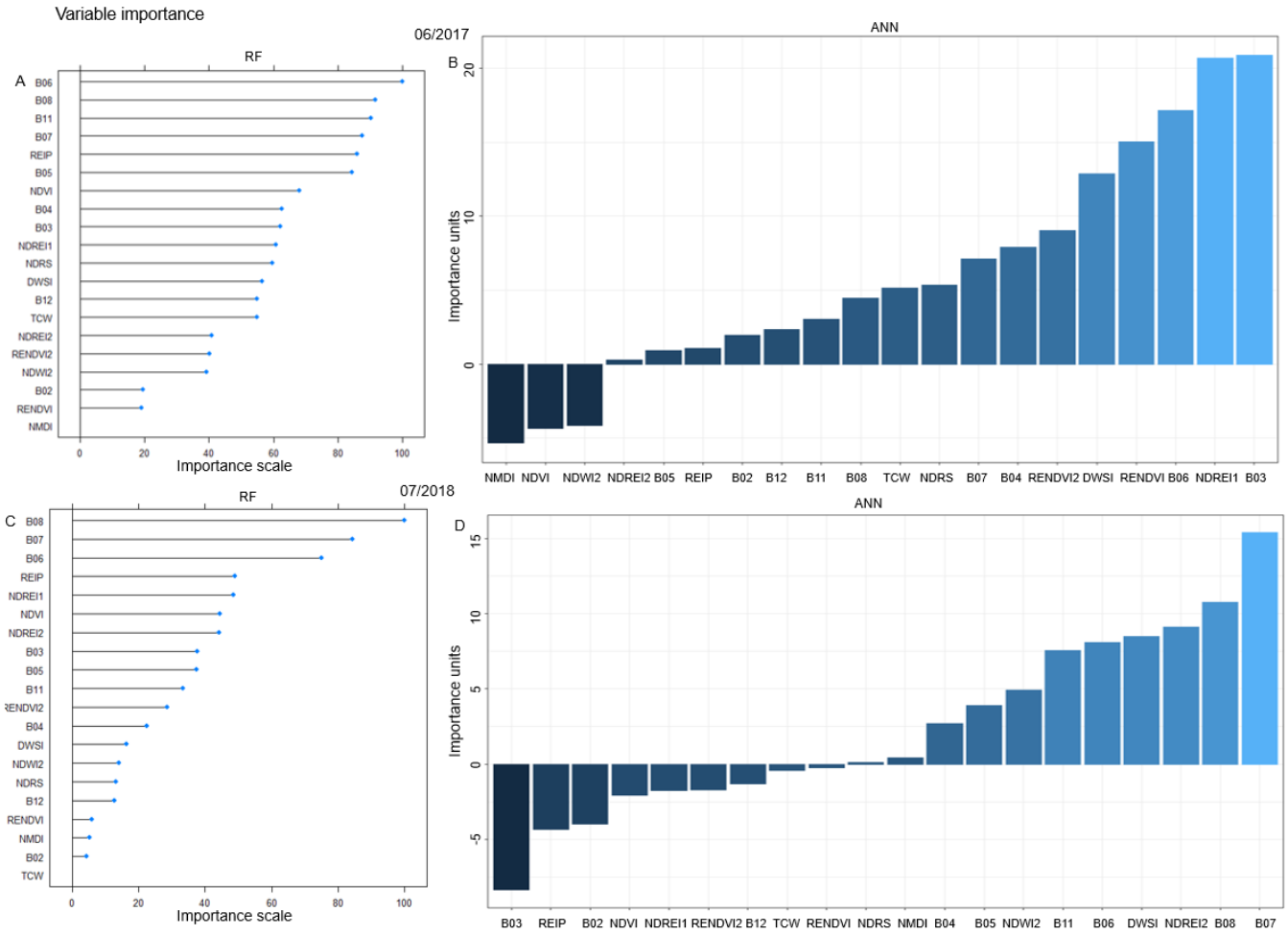

Figure 11. Variable importance for RF and ANN for two classification datasets (June 2017 (**A**,**B**) and July 2018 (**C**,**D**). Importance values for each explanatory variable for RF are expressed on a scale from 0 to 100 and were calculated with the R "caret" package (version 6.0.91). Variable importance for ANN was calculated with the R "NeuralNetTools" package (version 1.5.3) based on the relative importance of input variables in neural networks as the sum of the products of raw input–hidden and hidden–output connection weights, proposed by Olden et al. [55]. The importance values assigned to each variable are in units based directly on the summed product of the connection weights. The actual values should only be interpreted based on the relative sign and magnitude between explanatory variables, and comparisons between different models should be avoided [55].

3.3. Post-Classification Change Detection

Considering forest-cover changes that occurred in cropped areas 1 and 2 affected by both Vaia and bark beetle infestation damage, while the first change, represented in yellow, includes damages by both Vaia and bark beetles, the second change, represented in red, was caused only by bark beetle damage (Figure 12A,C). Cropped area 1 witnessed a change in forest cover of approximately 36% in the two years following the Vaia storm (Figure 12A), while cropped area 2 suffered a decrease in forest health of 65% from 2018 to 2020 (Figure 12C). As shown by the classification results and ground monitoring, we could confirm that both areas experienced an increase in bark beetle damage in the two years following the Vaia storm (mostly in 2020) compared to before the Vaia situation in 2018 (Figure 12B,D). In both cases, several forest stands were already suffering from stress in 2018, a year characterised by exceptionally high drought and low levels of precipitation [34,38], which led to a further increase in stressed canopies in 2019 (Figure 12B,D).

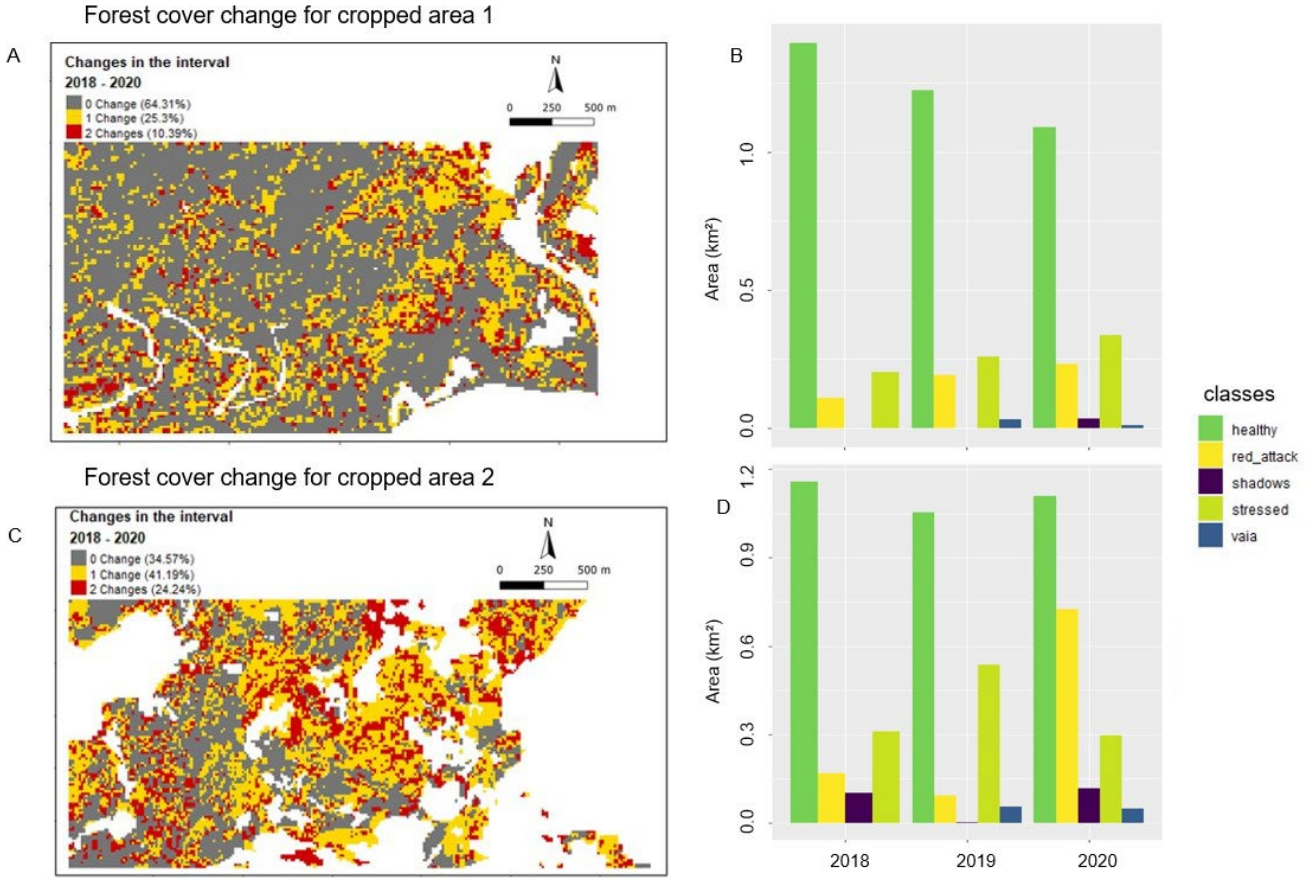

Figure 12. Forest-cover change maps in % (**A**) and (**C**) and land cover change per class in km² (**B**) and (**D**) for cropped areas 1 and 2 from 2018 to 2020 according to forest cover classes (healthy, red_attack, shadows, stressed and Vaia).

4. Discussion

According to the study results, Sentinel-2 data are suitable for the evaluation of forest health (forest condition before, during and after disturbance events), and the process of forest decline is detectable at the spatial resolution of a Sentinel-2 pixel. For this reason, the study areas represent a forest under different circumstances and development (Vaia storm damage, stressed forest stands, infested and dead trees after a bark beetle outbreak and forest vegetation without any significant influence). We could quantify an increase in forest loss after the Vaia storm, which triggered the outbreak of bark beetle populations (Figures 9, 10 and 12), also induced by increasing temperatures, low spring precipitation and drought, as indicated by climate reference data [28–34]. This scenario confirms that stands already suffering from biotic disturbances (e.g., bark beetles) are weakened and predisposed to suffer further damage from abiotic disturbances (e.g., windstorms and drought), which, again, trigger bark beetle infestations. This is consistent with previous studies [3,4,12,56].

The NIR (B08) and SWIR (B12) bands (Figure 5), as well as the vegetation indices NDWI, DWSI, NMDI, NDRS, NDREI, NDREI2 and especially TCW (Figure 6), were able to distinguish between healthy and stressed or damaged forest stands. The Red-Edge band (B06) and the NIR (B08) band exhibited the greatest potential for identifying stress and forest change during the classification process (Figure 11; Appendix A Figure A1 and A2). This can be explained by the fact that the Red-Edge and NIR parts of the electromagnetic spectrum are sensitive to changes in leaf pigments and canopy structure [15]. Red-Edge values were found to be helpful in estimating the chlorophyll concentrations as well as minimising the effects of background soil reflectance [23]. Furthermore, Red-Edge spectral reflectance indices should be used to increase the accuracy of mapping green-attacked

trees since they are less correlated with changes in the forest structure, needle age, leaf intercellular structure of air-to-cell wall interfaces, forest floor moisture content and tree physiology over the growing seasons in healthy forests [23]. Vegetation indices relying on the Red-Edge (B06 and B07), SWIR (B12) and red (B04) bands performed better in identifying stressed forests during classification (Figure 11; Appendix A Figure A1 and A2). Pixels covering forest stands in the bark beetle "red_attack" stage showed an increase in reflectance values in the red (B04) and SWIR (B12) bands (Figure 7). A reduction in chlorophyll decreases the spectral absorption in the visible region, resulting in higher reflectance, especially in the red band [57]. Further, bark beetle attacks are known to decrease the canopy water content [20], affecting the SWIR part of the spectrum by causing an increase in reflectance [46]. Previous studies indicate that reflectance changes in infested Norway spruce trees were observable, especially in the Red-Edge and SWIR regions for both leaf and canopy levels, and that spectral vegetation indices calculated from the Red-Edge and SWIR spectral bands were able to differentiate between healthy and infested trees earlier than the other indices [15,20,21].

The classification results showed a high mean overall accuracy (89%) (Appendix A Table A1) for forest stand stress detection and proved the suitability of Sentinel-2 image processing, as differences in reflectance in comparison to healthy forest stands can already be detected when there are no visible changes at the ground level. Pixels covering forest stands identified as being in the bark beetle "red_attack" stage already showed symptoms of stress in the previous season (Figures 5, 6, 9 and 10). Since spectral differences between healthy and stressed trees could very well exist without an ongoing bark beetle infestation, it is insufficient to conclude that the green-attack stage was successfully detected with our Sentinel-2 monitoring framework. The results of previous studies [24,58,59] indicate that spectral differences can already exist at the beginning of the vegetation season, before attacks, or even in previous years. The spectral difference existing before attacks may be related to weakness and stress, which make the trees vulnerable to the selection and then successful infestation by the bark beetles [24]. Indeed, a study has shown that these stress-induced spectral changes could be more efficient indicators of early infestations than green-attack symptoms [24]. Similar spectral trait variations observed for bark beetle attacks are produced by various other types of disturbances [60]. However, bark beetle spots develop at a certain speed that is greater than that of most abiotic stresses [61].

The availability of cloud-free Sentinel-2 images is essential for assessing bark beetle activity. Unfortunately, mountain areas are frequently cloud-covered in spring, and therefore, only two cloud-free images were found for May within the study period (Table 1). Actually, this period can be used as an initial reference, especially for forest stands already showing stress before being attacked later on in the season or for forest stands affected by infestation from the previous season. We assume that forest stands classified as in the "red_attack" stage in July include canopies attacked in the previous season and classified as stressed according to our classification results (Figures 9 and 10D,F), as well as trees newly infested by the first bark beetle generation, which, according to the PHENIPS model, starts swarming in May [42]. Stands suffering from the bark beetle "red_attack" stage in September (Figures 9 and 10E) likely correspond to infestations by the second bark beetle generation, which, according to the PHENIPS model, starts swarming in July [42]. A survey conducted in the southeastern US suggested the high activity of bark beetles in June, with observed signs of infestation and spots in August 2019, two months after the activity [61]. The period between mid-June and early July was found to be appropriate for mapping beetle-induced early stress in trees in Central Europe [21]. For this reason, for the early estimation of forest vulnerability, Sentinel-2 image processing in late spring and early summer is also of great use in detecting spectral differences related to the bark beetle green-attack stage or general conditions of weakness and stress in tree canopies, as they could later be selected and successfully infested by bark beetles or harmed by abiotic disturbances. This would theoretically give forest managers sufficient time to proceed with salvage logging [62]. However, due to the current high outbreak levels, it is not

feasible to monitor large areas in a timely manner [15], and costs for punctual sanitary cuts are not sustainable for the forest management sector, especially in mountain areas [1].

Including information about the forest stand structure (e.g., tree age and density) using auxiliary data, such as biomass maps, tree species maps and stand attribute tables [24], and relying only on pure Norway spruce forest stands rather than forest mixtures would most likely increase the accuracy of the overall results and, even more, the ability to detect early infestations. Furthermore, according to a previous study [63], the accuracy of infestation detection drastically decreases with the decreasing number of infested trees within a mixed pixel. A real qualitative change could already be caused by an improvement in the spectral or spatial resolution, as shown by the discussion of the results or the non-pixel but object-oriented approach, which analyses not only information from a given pixel but also the context in which it is located [64]. Despite that, the general aim of this research was to perform image processing in an area with a vast extent and including mixed spruce strands to test Sentinel-2's suitability for early stress detection and general forest-cover change detection over broad areas affected by abiotic and biotic disturbances. In addition to generating static bark beetle infestation maps, the spatial spread could also be predicted by including data such as wetness and brightness slopes, which improved the predictive ability of bark beetle infestation models in a recent study [65]. The proportion of stand borders exposed to the south and west should also be considered, as they are more susceptible to bark beetle attacks [8].

Furthermore, attacks frequently occur at sites with higher vegetation surface temperatures at the border of forest stands, where exposure to sunlight creates warmer conditions [20]. Accurate and high-resolution data on soil moisture and land surface temperature could significantly improve the predictive ability of bark beetle infestation models [66,67]. Therefore, interpolated SWI and LST data from currently available low-resolution open-access imagery and evapotranspiration data [68] and prediction models such as PHENIPS-TDEF [69] could be implemented. Information about solar radiation, rather than commonly used meteorological variables, since increasing canopy surface temperature was found at attacked stands, is also recommended as a future research direction for early bark beetle infestation detection [20,70].

5. Conclusions

This research confirmed that windstorms trigger bark beetle infestations, especially in relation to increasing temperatures and drought conditions caused by climate change. The multi-temporal remote sensing analysis conducted with Sentinel-2 data was useful for studying forest canopy trajectories according to their health status. Single bands, vegetation indices and supervised image classification could discriminate between areas affected by stress and bark beetles compared to those of healthy forest stands. Our results suggest that remote monitoring is suitable for providing spatial information about stressed stands, even in an early stage when there are no visible changes at the canopy level but changes can be detected in spectral signatures beyond the visible spectrum. Overall, the results obtained by processing a Sentinel-2 multi-temporal series confirmed its suitability for early stress detection in forest stands and the evaluation of forest-cover changes over vast areas affected by both abiotic and biotic disturbances. Still, there is a need for further research for the early and accurate detection of bark-beetle-attacked forest stands to distinguish infestations from other stress factors, which is mandatory for the operational application of remote monitoring to bark beetle control strategies on a large scale. Indeed, a regional-scale assessment of damage is crucial for planning any measure, such as trapping and sanitation felling or managing the landscape structure for containing the spread. In addition, the proposed multi-temporal monitoring framework for wind and bark beetle detection and damage mapping is an initial but necessary step for better understanding regional-scale population dynamics. Such action is crucial, considering that

abiotic and biotic disturbances are predicted to occur with an increasing frequency in the future due to the impacts of climate change.

Author Contributions: Conceptualisation, M.D., A.C. and M.D.G.; methodology, A.C., M.D.G., M.D. and E.T.; software, A.C. and M.D.G.; validation, E.T.; formal analysis, A.C., M.D.G., M.D. and E.T.; investigation, A.C., M.D.G., M.D. and E.T.; resources, A.C., M.D. and E.T.; data curation, A.C., E,T.; writing—original draft preparation, A.C., M.D.G. and E.T.; writing—review and editing, A.C., M.D.G., M.D. and E.T.; visualisation, A.C., M.D.G., M.D. and E.T.; supervision, E.T. All authors have read and agreed to the published version of the manuscript.

Funding: This research received no external funding.

Data Availability Statement: Data and code are available at: https://github.com/anna-candotti/bark_beetle_mapping_sentinel_2 (accessed on 10 November 2022).

Acknowledgements: We kindly thank the Regional Forestry Service and the Regional Agency for Rural Development (ERSA) of the Autonomous Region Friuli Venezia Giulia and the Carinthian Institute for Geographic Information Systems (KAGIS) for providing reference data regarding bark beetle traps and damage as well as wind-felled areas.

Conflicts of Interest: The authors declare no conflict of interest. The funders had no role in the design of the study; in the collection, analyses or interpretation of data; in the writing of the manuscript; or in the decision to publish the results.

Appendix A

Table A1. Confusion matrices and overall statistics for RF and ANN for each classification dataset.

06/2017 RF					
Confusion Matrix and Statistics					
		Reference			
	Prediction	healthy	red_attack	shadows	stressed
	healthy	24	1	0	0
	red_attack	0	31	0	3
	shadows	0	0	26	0
	stressed	1	1	0	32
Overall Statistics					
	Accuracy	0.9535			
	95% CI	(0.9015, 0.9827)			
	No-Information Rate	0.2713			
	p-Value (Acc > NIR)	$<2.2 \times 10^{-16}$			
	Kappa	0.9377			
06/2017 ANN					
Confusion Matrix and Statistics					
		Reference			
	Prediction	healthy	red_attack	shadows	stressed
	healthy	33	1	0	1
	red_attack	0	31	0	6
	shadows	0	0	26	0
	stressed	2	1	0	28
Overall Statistics					
	Accuracy	0.9147			
	95% CI	(0.8525, 0.9567)			

	No-Information Rate	0.2713			
	p-Value (Acc > NIR)	$<2.2 \times 10^{-16}$			
	Kappa	0.8859			
07/2018 RF					
Confusion Matrix and Statistics					
		Reference			
	Prediction	healthy	red_attack	shadows	stressed
	healthy	23	1	0	0
	red_attack	0	24	0	1
	shadows	0	0	23	0
	stressed	4	2	0	26
Overall Statistics					
	Accuracy	0.9231			
	95% CI	(0.854, 0.9662)			
	No-Information Rate	0.2596			
	p-Value (Acc > NIR)	$<2.2 \times 10^{-16}$			
	Kappa	0.8973			
07/2018 ANN					
Confusion Matrix and Statistics					
		Reference			
	Prediction	healthy	red_attack	shadows	stressed
	healthy	26	0	0	3
	red_attack	0	26	1	0
	shadows	0	0	22	0
	stressed	1	1	0	24
Overall Statistics					
	Accuracy	0.9423			
	95% CI	(0.8787, 0.9785)			
	No-Information Rate	0.2596			
	p-Value (Acc > NIR)	$<2.2 \times 10^{-16}$			
	Kappa	0.9229			
05/2019 RF					
Confusion Matrix and Statistics					
		Reference			
	Prediction	healthy	shadows	stressed	vaia
	healthy	23	0	1	0
	shadows	0	19	0	0
	stressed	0	0	23	0
	vaia	0	0	0	19
Overall Statistics					
	Accuracy	0.9882			
	95% CI	(0.9362, 0.9997)			

	No-Information Rate	0.2824			
	p-Value (Acc > NIR)	$<2.2 \times 10^{-16}$			
	Kappa	0.9843			
05/2019 ANN					
Confusion Matrix and Statistics					
		Reference			
	Prediction	healthy	shadows	stressed	vaia
	healthy	23	0	0	0
	shadows	0	19	0	0
	stressed	0	0	24	0
	vaia	0	0	0	19
Overall Statistics					
	Accuracy	1			
	95% CI	(0.9575, 1)			
	No-Information Rate	0.2824			
	p-Value (Acc > NIR)	$<2.2 \times 10^{-16}$			
	Kappa	1			
07/2019 RF					
Confusion Matrix and Statistics					
		Reference			
	Prediction	healthy	red_attack	shadows	stressed	vaia
	healthy	45	0	0	0	0
	red_attack	0	23	0	2	5
	shadows	0	0	10	0	0
	stressed	0	3	0	59	0
	vaia	0	2	0	0	8
Overall Statistics						
	Accuracy	0.9236				
	95% CI	(0.8703, 0.9588)				
	No-Information Rate	0.3885				
	p-Value (Acc > NIR)	$<2.2 \times 10^{-16}$				
	Kappa	0.894				
07/2019 ANN						
Confusion Matrix and Statistics						
		Reference				
	Prediction	healthy	red_attack	shadows	stressed	vaia
	healthy	27	1	0	1	0
	red_attack	0	21	0	1	2
	shadows	0	0	11	0	0
	stressed	2	3	0	32	1
	vaia	0	3	0	0	13
Overall Statistics						
	Accuracy	0.8814				

	95% CI	(0.809, 0.9366)				
	No-Information Rate	0.2881				
	p-Value (Acc > NIR)	$<2.2 \times 10^{-16}$				
	Kappa	0.8462				
09/2019 RF						
Confusion Matrix and Statistics						
		Reference				
	Prediction	healthy	red_attack	shadows	stressed	vaia
	healthy	25	0	0	1	0
	red_attack	1	17	0	2	1
	shadows	0	0	3	0	0
	stressed	1	0	0	24	0
	vaia	0	1	0	0	20
Overall Statistics						
	Accuracy	0.9271				
	95% CI	(0.8555, 0.9702)				
	No-Information Rate	0.2812				
	p-Value (Acc > NIR)	$<2.2 \times 10^{-16}$				
	Kappa	0.9042				
09/2019 ANN						
Confusion Matrix and Statistics						
		Reference				
	Prediction	healthy	red_attack	shadows	stressed	vaia
	healthy	24	4	0	2	0
	red_attack	2	12	0	3	0
	shadows	0	0	3	0	0
	stressed	1	1	0	21	0
	vaia	0	1	0	1	21
Overall Statistics						
	Accuracy	0.8438				
	95% CI	(0.7554, 0.9098)				
	No-Information Rate	0.2812				
	p-Value (Acc > NIR)	$<2.2 \times 10^{-16}$				
	Kappa	0.7939				
07/2020 RF						
Confusion Matrix and Statistics						
		Reference				
	Prediction	healthy	red_attack	shadows	stressed	vaia
	healthy	31	0	0	3	0
	red_attack	0	28	0	2	0
	shadows	0	0	43	2	0
	stressed	4	7	0	28	0
	vaia	0	0	0	0	7

Overall Statistics						
	Accuracy	0.8839				
	95% CI	(0.8227, 0.9297)				
	No-Information Rate	0.2774				
	p-Value (Acc > NIR)	$<2.2 \times 10^{-16}$				
	Kappa	0.8487				
07/2020 ANN						
Confusion Matrix and Statistics						
		Reference				
	Prediction	healthy	red_attack	shadows	stressed	vaia
	healthy	27	0	0	4	0
	red_attack	1	28	0	6	0
	shadows	0	0	43	6	0
	stressed	7	7	0	19	0
	vaia	0	0	0	0	7
Overall Statistics						
	Accuracy	0.8				
	95% CI	(0.7283, 0.8599)				
	No-Information Rate	0.2774				
	p-Value (Acc > NIR)	$<2.2 \times 10^{-16}$				
	Kappa	0.7389				

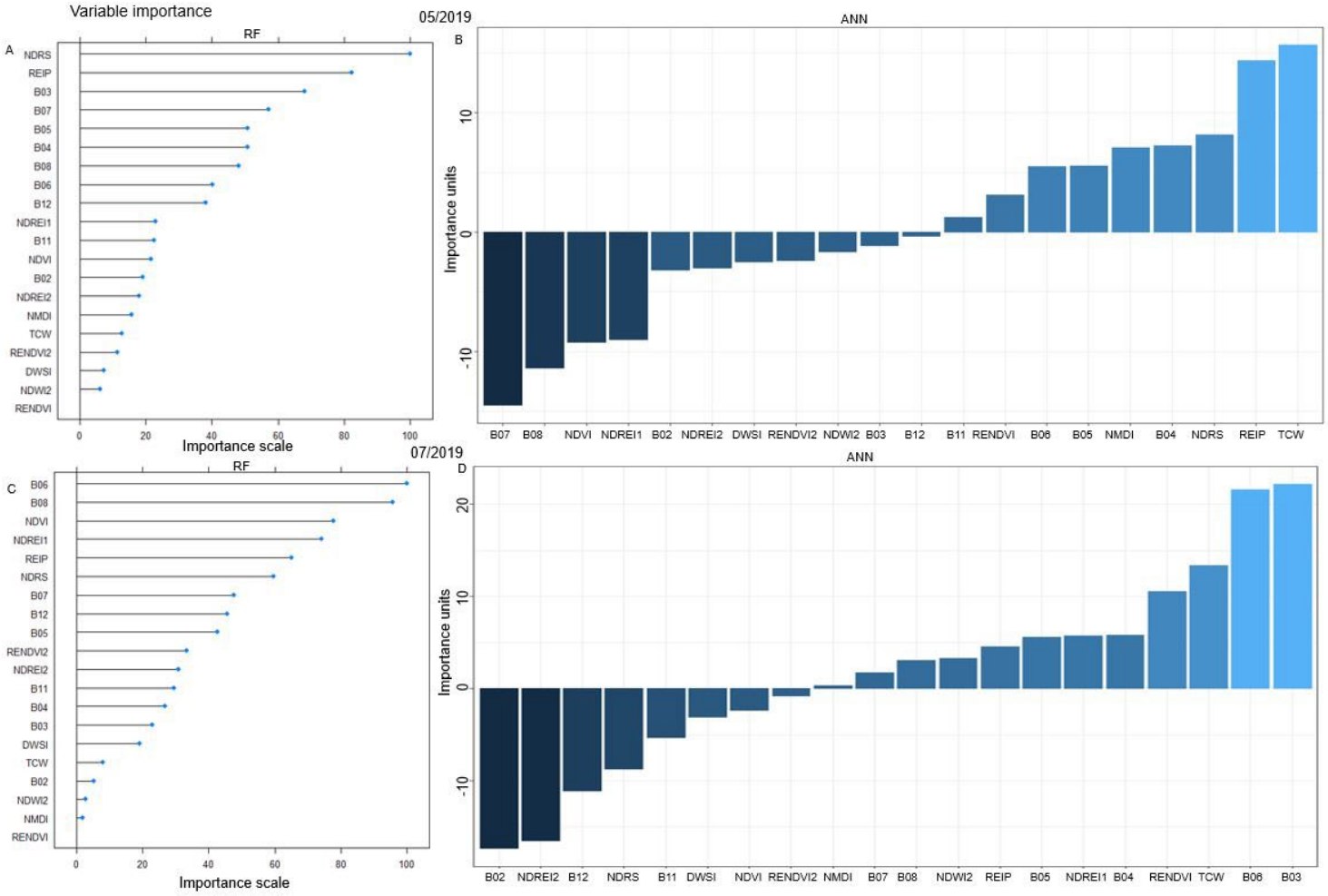

Figure A1. Variable importance for RF and ANN for classification datasets (May 2019 (**A**,**B**) and July 2019 (**C**,**D**)). Importance values for each explanatory variable for RF are expressed on a scale from 0 to 100 and were calculated with the R "caret" package (version 6.0.91). Variable importance for ANN was calculated with the R "NeuralNetTools" package (version 1.5.3) based on relative importance of input variables in neural networks as the sum of the products of raw input–hidden and hidden–output connection weights, proposed by Olden et al. [55]. The importance values assigned to each variable are in units that are based directly on the summed product of the connection weights. The actual values should only be interpreted based on relative sign and magnitude between explanatory variables. Comparisons between different models should not be made [55].

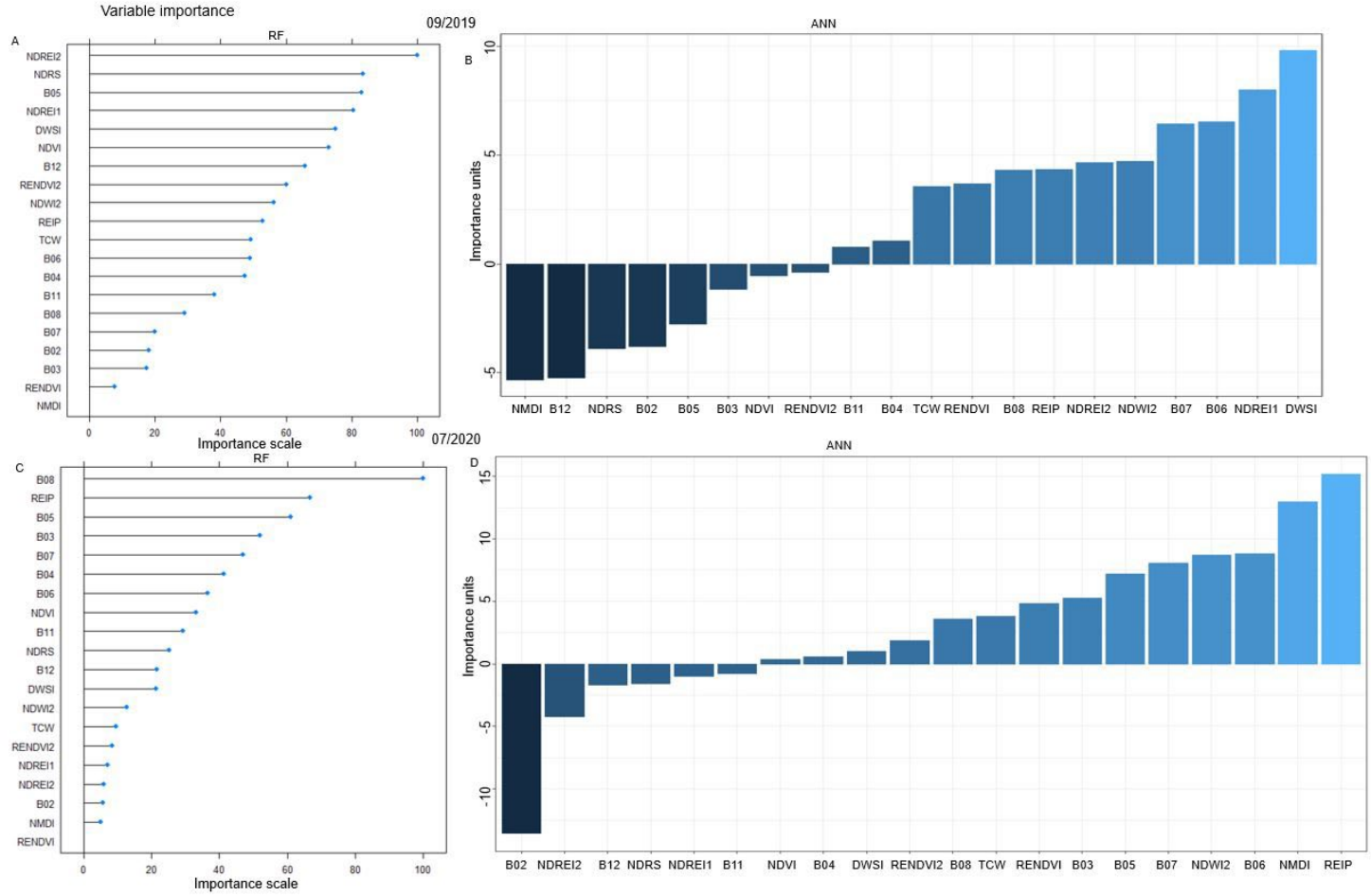

Figure A2. Variable importance for RF and ANN for classification datasets (September 2019 (**A**,**B**) and July 2020 (**C**,**D**)). Importance values for each explanatory variable for RF are expressed on a scale from 0 to 100 and were calculated with the R "caret" package (version 6.0.91). Variable importance for ANN was calculated with the R "NeuralNetTools" package (version 1.5.3) based on relative importance of input variables in neural networks as the sum of the products of raw input–hidden and hidden–output connection weights, proposed by Olden et al. [55]. The importance values assigned to each variable are in units that are based directly on the summed product of the connection weights. The actual values should only be interpreted based on relative sign and magnitude between explanatory variables. Comparisons between different models should not be made [55].

References

1. Gandhi, K.J.; Hofstetter, R.W. *Bark Beetle Management, Ecology and Climate Change*, 1st ed.; Academic Press: London, UK, 2021.
2. Niemann, K.O.; Quinn, G.; Stephen, R.; Visintini, F.; Parton, D. Hyperspectral Remote Sensing of Mountain Pine Beetle with an Emphasis on Previsual Assessment. *Can. J. Remote Sens.* **2015**, *41*, 191–202.
3. Seidl, R.; Thom, D.; Kautz, M.; Martin-Benito, D.; Peltoniemi, M.; Vacchiano, G.; Wild, J.; Ascoli, D.; Petr, M.; Honkaniemi, J.; et al. Forest disturbances under climate change. *Nat. Clim. Change* **2017**, *7*, 395–402.
4. Huang, J.; Kautz, M.; Trowbridge, A.M.; Hammerbacher, A.; Raffa, K.F.; Adams, H.D.; Goodsman, D.W.; Xu, C.; Meddens, A.J.; Kandasamy, D.; et al. Tree defense and bark beetles in a drying world: Carbon partitioning, functioning and modelling. *New Phytol.* **2020**, *225*, 26–36.
5. Montzka, C.; Bayat, B.; Tewes, A.; Mengen, D.; Vereecken, H. Sentinel-2 Analysis of Spruce Crown Transparency Levels and Their Environmental Drivers After Summer Drought in the Northern Eifel (Germany). *Front. For. Glob. Change* **2021**, *4*, 86.
6. Morris, J.L.; Cottrell, S.; Fettig, C.J.; Hansen, W.D.; Sherriff, R.L.; Carter, V.A.; Clear, J.L.; Clement, J.; DeRose, R.J.; Hicke, J.A.; et al. Managing bark beetle impacts on ecosystems and society: Priority questions to motivate future research. *J. Appl. Ecol.* **2017**, *54*, 750–760.
7. Dobor, L.; Hlásny, T.; Zimová, S. Contrasting vulnerability of monospecific and species-diverse forests to wind and bark beetle disturbance: The role of management. *Ecol. Evol.* **2020**, *10*, 12233–12245.

8. Wermelinger, B. Ecology and management of the spruce bark beetle *Ips typographus*—A review of recent research. *For. Ecol. Manag*. **2004**, *202*, 67–82.
9. Niemann, K.O.; Visintini, F. *Assessment of Potential for Remote Sensing Detection of Bark Beetle-Infested Areas during Green Attack: A Literature Review*; Mountain Pine Beetle Initiative Working Paper 2005-02; Natural Resources Canada, Canadian Forest Service, Pacific Forestry Centre: Victoria, BC, Canada, 2005.
10. White, J.; Wulder, M.; Brooks, D.; Reich, R.; Wheate, R. Detection of Red Attack Stage Mountain Pine Beetle Infestation with High Spatial Resolution Satellite Imagery. *Remote Sens. Environ*. **2005**, *96*, 340–351.
11. Wulder, M.A.; Dymond, C.C.; White, J.C.; Leckie, D.G.; Carroll, A.L. Surveying Mountain Pine Beetle Damage of Forests: A Review of Remote Sensing Opportunities. *For. Ecol. Manag*. **2006**, *221*, 27–41.
12. Hlásny, T.; König, L.; Krokene, P.; Lindner, M.; Montagné-Huck, C.; Müller, J.; Qin, H.; Raffa, K.F.; Schelhaas, M.-J.; Svoboda, M.; et al. Bark Beetle Outbreaks in Europe: State of Knowledge and Ways Forward for Management. *Curr. For. Rep*. **2021**, *7*, 138–165.
13. Lechner, A.M.; Foody, G.M.; Boyd, D.S. Applications in Remote Sensing to Forest Ecology and Management. *One Earth* **2020**, *2*, 405–412.
14. Fernandez-Carrillo, A.; Patočka, Z.; Dobrovolný, L.; Franco-Nieto, A.; Revilla-Romero, B. Monitoring Bark Beetle Forest Damage in Central Europe. A Remote Sensing Approach Validated with Field Data. *Remote Sens.* **2020**, *12*, 3634.
15. Bárta, V.; Lukeš, P.; Homolová, L. Early Detection of Bark Beetle Infestation in Norway Spruce Forests of Central Europe Using Sentinel-2. *Int. J. Appl. Earth Obs. Geoinf.* **2021**, *100*, 102335.
16. Senf, C.; Seidl, R.; Hostert, P. Remote Sensing of forest insect disturbances: Current state and future directions. *Int. J. Appl. Earth Obs. Geoinf.* **2017**, *60*, 49–60.
17. Zarco-Tejada, P.J.; Sepulcre-Cantó, G. Remote sensing of vegetation biophysical parameters for detecting stress condition and land cover changes. *Estud. Zona Saturada Suelo* **2007**, *8*, 37–44.
18. Carter, G.A. Primary and secondary effects of water content on the spectral reflectance of leaves. *Am. J. Bot.* **1991**, *78*, 916–924.
19. Einzmann, K.; Atzberger, C.; Pinnel, N.; Glas, C.; Böck, S.; Seitz, R.; Immitzer, M. Early detection of spruce vitality loss with hyperspectral data: Results of an experimental study in Bavaria, Germany. *Remote Sens. Environ.* **2021**, *266*, 112676.
20. Abdullah, H.; Skidmore, A.K.; Darvishzadeh, R.; Heurich, M. Sentinel-2 Accurately Maps Green-Attack Stage of European Spruce Bark Beetle (*Ips typographus*, L.) Compared with Landsat-8. *Remote Sens. Ecol. Conserv.* **2019**, *5*, 87–106.
21. Abdullah, H. Remote Sensing of European Spruce (*Ips typographus*, L.) Bark Beetle Green Attack. Ph.D. Thesis, University of Twente, Twente, The Netherlands, 2019.
22. Lastovicka, J.; Svec, P.; Paluba, D.; Kobliuk, N.; Svoboda, J.; Hladky, R.; Stych, P. Sentinel-2 Data in an Evaluation of the Impact of the Disturbances on Forest Vegetation. *Remote Sens.* **2020**, *12*, 1914.
23. Zabihi, K.; Surovy, P.; Trubin, A.; Singh, V.V.; Jakus, R. A review of major factors influencing the accuracy of mapping green-attack stage of bark beetle infestations using satellite imagery: Prospects to avoid data redundancy. *Remote Sens. Appl. Soc. Environ.* **2021**, *24*, 100638.
24. Huo, L.; Persson, H.J.; Lindberg, E. Early Detection of Forest Stress from European Spruce Bark Beetle Attack, and a New Vegetation Index: Normalized Distance Red & SWIR (NDRS). *Remote Sens. Environ.* **2021**, *255*, 112240.
25. Bernardinelli, I.; Stergulc, F.; Frigimelica, G.; Zandigiacomo, P.; Faccoli, M. Spatial analysis of *Ips typographus* Infestations in South-Eastern Alps. In Proceedings of the **7th Workshop on Methodology of Forest Insect and Disease Survey in Central Europe (**IUFRO Working Party 7.03.10**)**, Gmunden, Austria, 11–14 September 2006.
26. Del Favero, R. *La Vegetazione Forestale e la Silvicoltura Nella Regione Friuli Venezia Giulia*, 1st ed.; Colophon: Venezia, Italy, 1998.
27. Seger, M. *Waldschadensforschung im Gailtal, Kärnten. Erfassung des Waldzustandes mittels Farbinfrarot-Fernerkundung und Standort- Sowie Immissionsökologische Ansätze zur Ursachenforschung*; Carinthia II: Klagenfurt, Austria, 1994; pp. 555–625.
28. Regione Autonoma Friuli Venezia Giulia, Arpa, FVG. Available online: https://www.arpa.fvg.it/temi/temi/meteo-e-clima/sezioni-principali/clima-e-cambiamenti-climatici/clima/ (accessed on 7 July 2022).
29. ZAMG, Zentralanstalt für Meteorologie und Geodynamik. Available online: https://www.zamg.ac.at/cms/de/forschung/klima/klimatografien/klimaatlas-kaernten (accessed on 7 July 2022).
30. Unione Meteorologica del Friuli Venezia Giulia. Available online: https://www.umfvg.org/drupal/sites/default/files/Meteorologica-2019-01_02-compresso.pdf (accessed on 7 July 2022).
31. Regione Autonoma Friuli Venezia Giulia, Arpa, FVG. Available online: https://www.arpa.fvg.it/temi/temi/meteo-e-clima/news/e-online-il-report-meteofvg-dedicato-al-2019-un-anno-molto-caldo-con-piogge-abbondanti-in-autunno/ (accessed on 7 July 2022).
32. Regione Autonoma Friuli Venezia Giulia, Arpa, FVG. Available online: https://www.arpa.fvg.it/temi/temi/meteo-e-clima/news/2020-un-anno-caldo-con-piogge-eccezionali-a-dicembre-il-riepilogo-nel-report-annuale-meteofvg/ (accessed on 7 July 2022).
33. Faccoli, M. Effect of weather on *Ips typographus* (Coleoptera Curculionidae) phenology, voltinims, and associate spruce mortality in the southeastern Alps. *Environ. Entomol*. **2009**, *38*, 307–316.
34. Regione Autonoma Friuli Venezia Giulia, Arpa, FVG. Available online: https://www.meteo.fvg.it/pubblicazioni/meteo-fvg//2018/meteo.fvg_2018-5_it.pdf (accessed on 7 July 2022).
35. Chirici, G.; Giannetti, F.; Travaglini, D.; Nocentini, S.; Francini, S.; D'Amico, G.; Calvo, E.; Fasolini, D.; Broll, M.; Maistrelli, F.; et al. Stima dei danni della tempesta "Vaia" alle foreste in Italia. *Forest@* **2019**, *16*, 3–9.
36. Motta, R.; Ascoli, D.; Corona, P.; Marchetti, M.; Vacchiano, G. Selvicoltura e schianti da vento. Il caso della "tempesta Vaia". *Forest@* **2018**, *15*, 94–98.
37. European Space Agency. *Sentinel-2 Level-2A Algorithm Theoretical Basis Document*; European Space Agency: Paris, France, 2020.

38. European Space Agency. *Sentinel-2 User Handbook*; European Space Agency: Paris, France, 2015.
39. Regione Autonoma Friuli Venezia Giulia, Ersa, Bausinve 2020. Available online: http://www.ersa.fvg.it/export/sites/ersa/aziende/in-formazione/notiziario/allegati/2021/Inserto-Bausive-2020.pdf (accessed on 7 July 2022).
40. Copernicus Land Monitoring Service. Available online: https://land.copernicus.eu/ (accessed on 7 July 2022).
41. Regione Autonoma Friuli Venezia Giulia, Ersa, Bausinve 2019. Available online: http://ersa.regione.fvg.it/export/sites/ersa/aziende/in-formazione/notiziario/allegati/2020/1/BAUSINVE_2019.pdf (accessed on 7 July 2022).
42. Institut für Forstentomologie, Forstpathologie und Forstschutz. Monitoring und Risikoanalyse. Phenips Online Monitoring. Available online: https://ifff-server.boku.ac.at/wordpress/index.php/language/de/startseite/phenips-online/ (accessed on 7 July 2022).
43. Regione Autonoma Friuli Venezia Giulia, Irdat. Available online: http://irdat.regione.fvg.it/WebGIS/ (accessed on 7 July 2022).
44. NASA, Earthdata Search. Available online: https://search.earthdata.nasa.gov/search (accessed on 7 July 2022).
45. Copernicus Open Access Hub. Available online: https://scihub.copernicus.eu/dhus/#/home (accessed on 7 July 2022).
46. Gao, B.C. NDWI—A normalized difference water index for remote sensing of vegetation liquid water from space. *Remote Sens. Environ.* **1996**, *58*, 257–266.
47. Wang, L.; Qu, J.J. NMDI: A normalized multi-band drought index for monitoring soil and vegetation moisture with satellite remote sensing. *Geophys. Res. Lett.* **2007**, *34, L20405,* 1-5. https://doi.org/10.1029/2007GL031021.
48. Zbigniew, B.; Ziolkowski, D.; Bartold, M.; Orlowska, K.; Ochtyra, A. Monitoring forest biodiversity and the impact of climate on forest environment using high-resolution satellite images. *Eur. J. Remote Sens.* **2018**, *51*, 166–181.
49. Chen, G.; Meentemeyer, R.K. Remote Sensing of Forest Damage by Diseases and Insects. In *Remote Sensing for Sustainability*; Weng, Q., Ed.; CRC Press: Boca Raton, FL, USA; 2016; pp. 145–157.
50. Evangelides, C.; Nobajas, A. Red-Edge Normalised Difference Vegetation Index (NDVI705) from Sentinel-2 imagery to assess post-fire regeneration. *Remote Sens. Appl. Soc. Environ.* **2020**, *17*, 100283.
51. Cundill, S.L.; Van der Werff, H.M.; Van der Meijde, M. Adjusting Spectral Indices for Spectral Response Function Differences of Very High Spatial Resolution Sensors Simulated from Field Spectra. *Sensors* **2015**, *15*, 6221–6240.
52. Index Database. A database for remote sensing indices. Available online: www.indexdatabase.de (accessed on 07 July 2020).
53. Clark Labs, Clark University, TerrSet Manual. Available online: https://clarklabs.org/wp-content/uploads/2016/10/Terrset-Manual.pdf (accessed on 07 July 2020).
54. Aldwaik, S.Z.; Pontius, R.G. Jr. Intensity analysis to unify measurements of size and stationarity of land changes by interval, category and transition. *Landsc. Urban Plan.* **2012**, *106*, 103–114.
55. Olden, J.D.; Joy, M.K.; Death, R.G. An accurate comparison of methods for quantifying variable importance in artificial neural networks using simulated data. *Ecol. Model.* **2004**, *178*, 389–397.
56. Ochtyra, A. Forest Disturbances in Polish Tatra Mountains for 1985–2016 in Relation to Topography, Stand Features, and Protection Zone. *Forests* **2020**, *11*, 579.
57. Carter, G.A.; Knapp, A.K. Leaf optical properties in higher plants: Linking spectral characteristics to stress and chlorophyll concentration. *Am. J. Bot*. **2001**, *88*, 677–684.
58. Abdollahnejad, A.; Panagiotidis, D.; Surový, P.; Modlinger, R. Investigating the Correlation between Multisource Remote Sensing Data for Predicting Potential Spread of Ips typographus L. Spots in Healthy Trees. Remote Sens. **2021**, *13*, 4953.
59. Lausch, A.; Heurich, M.; Dordalla, D.; Dobner, H.J.; Gwillym-Margianto, S.; Salbach, C. Forecasting potential bark beetle outbreaks based on spruce forest vitality using hyperspectral remote-sensing techniques at different scales. *For. Ecol. Manag.* **2013**, *308*, 76–89.
60. Lausch, A.; Erasmi, S.; King, D.J.; Magdon, P.; Heurich, M. Understanding forest health with remote sensing—Part I—A review of spectral traits, processes and remote-sensing characteristics. *Remote Sens.* **2016**, *8*, 1029.
61. Gomez, D.F.; Ritger, H.M.W.; Pearce, C.; Eickwort, J.; Hulcr, J. Ability of Remote Sensing Systems to Detect Bark Beetle Spots in the Southeastern US. *Forests* **2020**, *11*, 1167.
62. *Faccoli, M.; Finozzi, V.; Andriolo, A.; Bernardinelli, I.; Salvadori, C.; Deganutti, L.; Battisti, A. Il bostrico tipografo sulle Alpi orientali. Evoluzione, gestione e prospettive future dopo Vaia. Sherwood For. Alberi Oggi* **2022**, *257, 23–26.*
63. Meddens, A.J.H.; Hicke, J.A.; Vierling, L.A.; Hudak, A.T. Evaluating methods to detect bark beetle-caused tree mortality using single-date and multi-date Landsat imagery. *Remote Sens. Environ.* **2013**, *132*, 49–58.
64. Migas-Mazur, R.; Kycko, M.; Zwijacz-Kozica, T.; Zagajewski, B. Assessment of Sentinel-2 Images, Support Vector Machines and Change Detection Algorithms for Bark Beetle Outbreaks Mapping in the Tatra Mountains. *Remote Sens*. **2021**, *13*, 3314.
65. Hais, M.; Wild, J.; Berec, L.; Bruna, J.; Kennedy, R.; Braaten, J.; Broz, Z. Landsat imagery spectral-trajectories—Important variables for spatially predicting the risks of bark beetle disturbance. *Remote Sens*. **2016**, *8*, 687.
66. Hais, M.; Kucera, T. Surface temperature change of spruce forest as a result of bark beetle attack: Remote sensing and GIS approach. *Eur. J. For. Res.* **2008**, *127*, 327–337.
67. Nardi, D.; Jactel, H.; Pagot, E.; Samalens, J.C.; Marini, L. Drought and stand susceptibility to attacks by the European spruce bark beetle: A remote sensing approach. *Agric. For. Entomol.* **2022**, 1–11. https://doi.org/10.1111/afe.12536.
68. Knowles, J.F.; Molotoch, N.P. *Bark Beetle Impacts on Remotely Sensed Evapotranspiration in the Colorado Rocky Mountains*; Colorado Water Institute: Collins, CO, USA, 2019.

69. Institut für Forstentomologie, Forstpathologie und Forstschutz. Monitoring und Risikoanalyse. Phenips-TDEF—Der Einfluss von Trockenperioden auf das Befallsrisiko durch Buchdrucker. Available online: PHENIPS-TDEF | https://ifff-server.boku.ac.at/wordpress/index.php/home/phenips-tdef/ (accessed on 7 July 2022).
70. Mezei, P.; Potterf, M.; Skvarenina, J.; Rasmussen, J.G.; Jakus, R. Potential Solar Radiation as a Driver for Bark Beetle Infestation on a Landscape Scale. *Forests* **2019**, *10*, 604.